Searches for transverse momentum dependent flow vector fluctuations in Pb-Pb and p-Pb collisions at the LHC

(ALICE Collaboration) Acharya, S.; ...; Antičić, Tome; ...; Erhardt, Filip; ...; Gotovac, Sven; ...; Jerčić, Marko; ...; ...

Source / Izvornik: **Journal of High Energy Physics, 2017, 2017**

Journal article, Published version
Rad u časopisu, Objavljena verzija rada (izdavačev PDF)

https://doi.org/10.1007/JHEP09(2017)032

Permanent link / Trajna poveznica: https://urn.nsk.hr/urn:nbn:hr:217:403959

Rights / Prava: Attribution 4.0 International/Imenovanje 4.0 međunarodna

Download date / Datum preuzimanja: **2024-03-29**



Repository / Repozitorij:

Repository of the Faculty of Science - University of Zagreb





Published for SISSA by Springer

Received: *July 19, 2017*
Accepted: *August 5, 2017*
Published: *September 8, 2017*

Searches for transverse momentum dependent flow vector fluctuations in Pb–Pb and p–Pb collisions at the LHC



The ALICE collaboration

E-mail: ALICE-publications@cern.ch

Abstract: The measurement of azimuthal correlations of charged particles is presented for Pb–Pb collisions at $\sqrt{s_{\rm NN}} = 2.76\,\text{TeV}$ and p–Pb collisions at $\sqrt{s_{\rm NN}} = 5.02\,\text{TeV}$ with the ALICE detector at the CERN Large Hadron Collider. These correlations are measured for the second, third and fourth order flow vector in the pseudorapidity region $|\eta| < 0.8$ as a function of centrality and transverse momentum $p_{\rm T}$ using two observables, to search for evidence of $p_{\rm T}$-dependent flow vector fluctuations. For Pb–Pb collisions at 2.76 TeV, the measurements indicate that $p_{\rm T}$-dependent fluctuations are only present for the second order flow vector. Similar results have been found for p–Pb collisions at 5.02 TeV. These measurements are compared to hydrodynamic model calculations with event-by-event geometry fluctuations in the initial state to constrain the initial conditions and transport properties of the matter created in Pb–Pb and p–Pb collisions.

Keywords: Heavy Ion Experiments

ArXiv ePrint: 1707.05690

Open Access, Copyright CERN,
for the benefit of the ALICE Collaboration.
Article funded by SCOAP^3.

https://doi.org/10.1007/JHEP09(2017)032

JHEP09(2017)032

Contents

1 Introduction **1**

2 Probes of p_{T}-dependent flow vector fluctuations **3**

3 Experimental setup **4**

4 Event and track selection **5**

5 Systematic uncertainties **6**

6 Results and discussion **7**

6.1 Pb–Pb collisions 7

6.2 p–Pb collisions 16

7 Summary **19**

The ALICE collaboration **26**

JHEP09(2017)032

1 Introduction

The primary goal of ultrarelativistic heavy-ion collisions is to study the properties of the Quark-Gluon Plasma (QGP), a state of matter predicted by Quantum Chromodynamics to exist at high temperatures and energy densities [1, 2]. An important experimental observable used to accomplish this goal is the azimuthal anisotropy of particles emitted in the transverse plane. In non-central heavy-ion collisions, the overlap region of the Lorentz-contracted nuclei is roughly almond-shaped. Nucleons contained in such anisotropic overlap region interact with each other and give rise to a system of high energy density which expands anisotropically. These interactions convert the initial spatial asymmetry into a final-state momentum anisotropy of the produced particles, a phenomenon referred to as collective anisotropic flow [3–5]. Anisotropic flow is characterised using a Fourier decomposition of the azimuthal distribution of particles with respect to the flow symmetry planes [6, 7]

$$E\frac{\mathrm{d}^3N}{\mathrm{d}^3\vec{p}} = \frac{1}{2\pi}\frac{\mathrm{d}^2N}{p_{\mathrm{T}}\mathrm{d}p_{\mathrm{T}}\mathrm{d}\eta}\left(1+2\sum_{n=1}^{\infty}v_n\cos[n(\varphi-\Psi_n)]\right), \tag{1.1}$$

where N is the number of produced particles, E is the energy, $\vec{p}$ the momentum, p_{T} the transverse momentum, φ the azimuthal angle and η the pseudorapidity of the particle. The n^{th} order flow (vector) V_n is defined as: $V_n \equiv v_n\, e^{in\Psi_n}$, where v_n is the flow coefficient, and Ψ_n represents the azimuth of V_n in momentum space (flow angle). For a uniform matter distribution in the initial stage of a heavy-ion collision, Ψ_n for $n \geq 1$ coincides with the reaction plane defined by the beam direction and impact parameter. Due to event-by-event fluctuations of the participating nucleons distribution inside the overlap region, the Ψ_n may

deviate from the reaction plane and the odd flow coefficients v_{2n-1} are non-vanishing [8–14]. Large flow coefficients were observed at the Relativistic Heavy-Ion Collider (RHIC) [15–18] and the Large Hadron Collider (LHC) [19–29]. These measurements constrain the initial conditions (e.g. energy and entropy density) and transport coefficients of the system (such as shear viscosity over entropy density ratio, η/s). The recent measurements of correlations between different order flow coefficients and flow angles [23, 30], together with the comparisons to theoretical calculations, indicate that the matter created in ultrarelativistic heavy-ion collisions behaves as a nearly perfect fluid (almost zero η/s) whose constituent particles interact strongly [31].

Traditionally the final-state symmetry plane angles are estimated event-by-event from the particle azimuthal distribution over a large range in p_{T}. However, hydrodynamic calculations indicate a p_{T} dependence of the flow vector V_n due to event-by-event fluctuations in the initial energy density of the nuclear collisions [32, 33]. These flow vector fluctuations could be responsible for the experimentally observed breakdown of the factorisation [25, 27, 34]. They might also affect the measured p_{T}-differential anisotropic flow $v_n(p_{\mathrm{T}})$ [33]. Therefore, searches for p_{T}-dependent flow vector fluctuations become important and these measurements together with the comparisons to theoretical calculations not only constrain the transport properties, but also shed light on the initial conditions in heavy-ion collisions.

Studies of azimuthal correlations are performed also in p–Pb collisions at the LHC. The original goal of p–Pb collisions was to provide reference data for the high energy Pb–Pb collisions. However, indications of collective behaviour have been discovered by the ALICE, ATLAS, CMS and LHCb collaborations [35–46]. If the azimuthal correlations in small collision systems reveal the onset of hydrodynamic flow behaviour, the breakdown of factorisation should be expected in small collision systems and reproduced by hydrodynamic calculations as well.

The first experimental indication of p_{T}-dependent flow vector fluctuations was observed by ALICE in studies of the decomposition of Fourier harmonics of the two-particle azimuthal correlations [34]. Fits to the azimuthal correlations, assuming factorisation of the two-particle Fourier harmonics, agree well with data up to $p_{\mathrm{T}}^{a} \sim 3$–$4\,\mathrm{GeV}/c$, deviations at higher p_{T} are interpreted, as at least partially, due to away-side recoil jet contributions [34]. A systematic study of the factorisation of long-range two-particle Fourier harmonic into the flow coefficients is also performed in both Pb–Pb and p–Pb collisions by CMS [41, 47].

In this paper, the p_{T}-dependent flow vector fluctuations are investigated in more detail using novel observables for azimuthal correlations, for charged particles in Pb–Pb collisions at $\sqrt{s_{\mathrm{NN}}} = 2.76\,\mathrm{TeV}$ and p–Pb collisions at $\sqrt{s_{\mathrm{NN}}} = 5.02\,\mathrm{TeV}$ with the ALICE detector. The definitions of the observables are given in section 2. The experimental setup is described in section 3. The results are reported in multiple centrality classes for Pb–Pb collisions and multiplicity classes for p–Pb collisions for several transverse momentum intervals. Details of the event and track selections are given in section 4. Section 5 shows the study of systematic uncertainties of the aforementioned observables. Section 6 presents results and discussions while section 7 summarizes and concludes this work.

JHEP09(2017)032

2 Probes of p_{T}-dependent flow vector fluctuations

The traditional approach used to measure anisotropic azimuthal correlations is as follows: first, the flow coefficient of reference particles (RPs), called reference flow, is determined over a wide kinematic range, and then the transverse momentum differential flow coefficient is calculated by correlating the particles of interest (POIs) with respect to the reference flow obtained in the first step. Usually a pseudorapidity gap $|\Delta\eta|$ is applied between the two correlated particles to suppress non-flow effects, which comprise azimuthal correlations not associated with flow symmetry planes, e.g. resonance decays and jet contributions. This approach has commonly been used to measure the anisotropic flow at the LHC [20, 25, 28]. Considering possible p_{T}-dependent flow angle and/or magnitude fluctuations and neglecting non-flow contributions, the flow coefficient from p_{T} interval a measured with 2-particle correlations can be expressed as

$$v_n\{2\}(p_{\mathrm{T}}^a) = \frac{\langle\langle\cos\left[n\left(\varphi_1^a - \varphi_2^{\mathrm{ref}}\right)\right]\rangle\rangle}{\sqrt{\langle\langle\cos\left[n\left(\varphi_1^{\mathrm{ref}} - \varphi_2^{\mathrm{ref}}\right)\right]\rangle\rangle}} = \frac{\langle v_n(p_{\mathrm{T}}^a)\, v_n^{\mathrm{ref}}\, \cos\left[n\left(\Psi_n(p_{\mathrm{T}}^a) - \Psi_n\right)\right]\rangle}{\sqrt{\langle {v_n^{\mathrm{ref}}}^2\rangle}}. \quad (2.1)$$

Here, a single set of angular brackets denotes averaging over events, and a double set indicates averaging over both particles and events. The φ^{ref} and φ^a represent the azimuthal angle of RPs and POIs, respectively. The v_n^{ref} stands for the reference flow, and $\Psi_n(p_{\mathrm{T}}^a)$ denotes the p_{T} differential symmetry plane angle at p_{T}^a, which might fluctuate around the p_{T} integrated symmetry plane angle Ψ_n. The cosine term $\langle\cos\left[n\left(\Psi_n(p_{\mathrm{T}}^a) - \Psi_n\right)\right]\rangle$ shows the effects of the difference between $\Psi_n(p_{\mathrm{T}})$ and Ψ_n, due to the p_{T}-dependent flow angle fluctuations. Additionally, $\langle v_n(p_{\mathrm{T}}^a)\, v_n^{\mathrm{ref}}\rangle$ cannot be factorised into the product of $\sqrt{\langle v_n(p_{\mathrm{T}}^a)^2\rangle}$ and $\sqrt{\langle {v_n^{\mathrm{ref}}}^2\rangle}$ if there are p_{T}-dependent flow coefficient fluctuations.

A new type of two-particle azimuthal correlations from p_{T}^a, denoted as $v_n[2](p_{\mathrm{T}}^a)$, is proposed in [33]:

$$\begin{aligned} v_n[2](p_{\mathrm{T}}^a) =& \sqrt{\langle\langle\cos\left[n\left(\varphi_1^a - \varphi_2^a\right)\right]\rangle\rangle} \\ =& \sqrt{\langle\langle\cos\left[n(\varphi_1^a - \Psi_n(p_{\mathrm{T}}^a)) - n\left(\varphi_2^a - \Psi_n(p_{\mathrm{T}}^a)\right)\right]\rangle\rangle} \\ =& \sqrt{\langle v_n(p_{\mathrm{T}}^a)^2\rangle}. \end{aligned} \quad (2.2)$$

The difference between $v_n\{2\}(p_{\mathrm{T}}^a)$ and $v_n[2](p_{\mathrm{T}}^a)$ is that the former takes the flow of RPs from a wide p_{T} range and the POIs from a certain p_{T} interval, while the latter is essentially the reference flow calculated within a narrow p_{T} range. The ratio of $v_n\{2\}$ and $v_n[2]$ allows p_{T}-dependent flow vector fluctuations

$$\frac{v_n\{2\}}{v_n[2]}(p_{\mathrm{T}}^a) = \frac{\langle v_n(p_{\mathrm{T}}^a)\, v_n^{\mathrm{ref}}\, \cos\left[n\left(\Psi_n(p_{\mathrm{T}}^a) - \Psi_n\right)\right]\rangle}{\sqrt{\langle v_n(p_{\mathrm{T}}^a)^2\rangle}\sqrt{\langle {v_n^{\mathrm{ref}}}^2\rangle}}. \quad (2.3)$$

When the correlations are dominated by flow, a ratio value smaller than unity shall indicate the presence of p_{T}-dependent flow vector fluctuations.

JHEP09(2017)032

Another observable to probe the p_{T}-dependent flow vector fluctuations is the factorisation ratio r_n [32, 33]. It can be calculated using the two-particle Fourier harmonic as

$$r_n = \frac{V_{n\Delta}(p_{\mathrm{T}}^a, p_{\mathrm{T}}^t)}{\sqrt{V_{n\Delta}(p_{\mathrm{T}}^a, p_{\mathrm{T}}^a)\, V_{n\Delta}(p_{\mathrm{T}}^t, p_{\mathrm{T}}^t)}}, \tag{2.4}$$

where $V_{n\Delta}(p_{\mathrm{T}}^a, p_{\mathrm{T}}^t)$ is the n^{th}-order Fourier harmonic of the two-particle azimuthal correlations of triggered and associated particles from p_{T}^t and p_{T}^a, and is calculated as

$$V_{n\Delta}(p_{\mathrm{T}}^a, p_{\mathrm{T}}^t) = \langle\langle \cos\left[n\left(\varphi_1^a - \varphi_2^t\right)\right]\rangle\rangle = \langle v_n(p_{\mathrm{T}}^a)\, v_n(p_{\mathrm{T}}^t)\, \cos\left[n(\Psi_n(p_{\mathrm{T}}^a) - \Psi_n(p_{\mathrm{T}}^t))\right]\rangle, \tag{2.5}$$

where $\Psi_n(p_{\mathrm{T}}^a)$ and $\Psi_n(p_{\mathrm{T}}^t)$ represent the flow angles at p_{T}^a and p_{T}^t, respectively. The subscript $_\Delta$ indicates that a pseudorapidity gap is usually applied to minimise contamination from non-flow effects. If both triggered and associated particle are from the same p_{T} interval p_{T}^t, eq. (2.5) reduces to

$$V_{n\Delta}(p_{\mathrm{T}}^a, p_{\mathrm{T}}^a) = \langle\langle \cos\left[n\left(\varphi_1^a - \varphi_2^a\right)\right]\rangle\rangle = \langle v_n(p_{\mathrm{T}}^a)^2\rangle. \tag{2.6}$$

Similarly, we have

$$V_{n\Delta}(p_{\mathrm{T}}^t, p_{\mathrm{T}}^t) = \langle\langle \cos\left[n\left(\varphi_1^t - \varphi_2^t\right)\right]\rangle\rangle = \langle v_n(p_{\mathrm{T}}^t)^2\rangle\,. \tag{2.7}$$

In the end r_n is equivalent to

$$r_n = \frac{\langle v_n(p_{\mathrm{T}}^a)\, v_n(p_{\mathrm{T}}^t)\, \cos\left[n(\Psi_n(p_{\mathrm{T}}^a) - \Psi_n(p_{\mathrm{T}}^t))\right]\rangle}{\sqrt{\langle v_n(p_{\mathrm{T}}^a)^2\rangle \langle v_n(p_{\mathrm{T}}^t)^2\rangle}}. \tag{2.8}$$

It can be seen that $r_n = 1$ does not always hold true, i.e. most of the known sources of non-flow effects do not factorise at low p_{T}, which is confirmed by Monte Carlo studies [48]. In a flow-dominated system, $r_n \leq 1$ due to the Cauchy-Schwarz inequality. Factorisation implies $r_n = 1$, while $r_n < 1$ shows the breaking of factorisation, suggesting the presence of p_{T}-dependent flow vector fluctuations [32, 33].

Note that eqs. (2.3) and (2.8) look very similar. The ratios $v_n\{2\}/v_n[2]$ include the p_{T} integrated information and probe the p_{T}-differential flow vector with respect to the p_{T} integrated flow vector. The r_n carries more detailed information on the 2-particle correlation structure for triggered and associated particle from narrow p_{T} intervals, and probe the fluctuations of flow vector at p_{T}^a and p_{T}^t; however, it also has larger statistical uncertainties. If the triggered particles are selected from a very wide kinematic range, the observable r_n becomes identical with $v_n\{2\}/v_n[2]$. In this paper, we study $v_n\{2\}/v_n[2]$ up to $n = 4$ and r_n up to $n = 3$.

3 Experimental setup

A Large Ion Collider Experiment (ALICE) [49] is the dedicated heavy-ion experiment at the LHC designed to study strongly interacting matter at extreme energy densities. It was built to cope with the large charged-particle multiplicity density in central Pb–Pb collisions at

JHEP09(2017)032

the LHC, with several thousand tracks per unit of pseudorapidity. The ALICE apparatus consists of a central barrel that measures hadrons, electrons, muons and photons, and a forward spectrometer for the identification of muons. Several smaller detectors in the forward region are used for triggering and global event characterization. The central barrel is located inside a solenoidal magnet that provides a magnetic field of up to 0.5 T. Charged tracks are reconstructed using the Time Projection Chamber (TPC) [49, 50] and the Inner Tracking System (ITS) [49, 51] with a track momentum resolution better than 2% for the momentum range $0.2 < p_{\mathrm{T}} < 5.0\,\mathrm{GeV}/c$ [52]. The TPC is the main tracking detector of the central barrel, sufficient with full azimuthal coverage in the range of $|\eta| < 0.9$. The ITS consists of six layers of silicon detectors placed at radii between 3.9 cm and 43 cm and matching the pseudorapidity acceptance of the TPC. Three different technologies are employed in the ITS: the two innermost layers are equipped with Silicon Pixel Detectors (SPD), the following two layers have Silicon Drift Detectors (SDD) and the two outer layers are double-sided Silicon Strip Detectors (SSD). The V0 detector [49, 53] was used for triggering and the determination of the event centrality. It consists of two arrays called V0-A and V0-C, each built from 32 scintillator counters and providing full azimuthal coverage, positioned on each side of the interaction point. The V0-A is situated at $z = 3.4\,\mathrm{m}$ ($2.8 < \eta < 5.1$) and the V0-C is located at $z = -0.9\,\mathrm{m}$ ($-3.7 < \eta < -1.7$). Each V0 counter provides the signal amplitude and timing information with a time resolution better than 1 ns [49, 53]. Two Zero Degree Calorimeters (ZDCs) [49] were used in the offline event selection. The ZDCs are a pair of hadronic calorimeters, one for detecting non-interacting neutrons (ZN) and one for spectator protons (ZP), located at 112.5 m on either side of the interaction point.

4 Event and track selection

The data samples analyzed in this article were recorded by ALICE during the 2010 Pb–Pb and 2013 p–Pb runs of the LHC at centre-of-mass energies of $\sqrt{s_{\mathrm{NN}}} = 2.76\,\mathrm{TeV}$ and $\sqrt{s_{\mathrm{NN}}} = 5.02\,\mathrm{TeV}$, respectively. The Pb–Pb run had equal beam energies, while the p–Pb run had beam energies of 4 TeV for protons and 1.58 TeV per nucleon for lead nuclei, which resulted in a rapidity shift of -0.465 of the centre-of-mass system with respect to the ALICE laboratory system. In the following, all kinematic variables are reported in the laboratory system. Minimum bias Pb–Pb and p–Pb events were triggered by the coincidence of signals in both V0 detectors. The trigger efficiency is 99.7% for non-diffractive Pb–Pb collisions [54] and 99.2% for non-single-diffractive p–Pb collisions [55]. Beam background events were rejected in an offline event selection for all data samples using the timing information from the V0 and ZDC detectors and by correlating reconstructed SPD clusters and tracklets. The remaining beam background was found to be smaller than 0.1% and was neglected. More details about the offline event selection can be found in [52]. The fraction of pile-up events in the data sample is found to be negligible after applying dedicated pile-up removal criteria [52]. Only events with a reconstructed primary vertex within $|z_{\mathrm{vtx}}| < 10$ cm with respect to the nominal interaction point were selected. The position of the primary vertex was estimated using tracks reconstructed by the ITS and

JHEP09(2017)032

TPC. The Pb–Pb collision centrality was determined from the measured V0 amplitude distribution [54]. The dataset of p–Pb collisions is divided into several multiplicity classes defined as fractions of the analysed event sample, based on the charge deposition in the V0-A detector. These multiplicity classes are denoted as "0–20%", "20–40%", "40–60%", and "60–100%", from the highest to the lowest multiplicity. About 13 million Pb–Pb and 92 million p–Pb minimum bias events passed all event selection criteria.

This analysis used tracks that were reconstructed based on the combined information from the TPC and ITS detectors. Primary charged tracks were required to have a distance of closest approach to the primary vertex in the longitudinal (z) direction and transverse (xy) plane smaller than 3.2 cm and 2.4 cm, respectively. Tracks with $0.2 < p_{\mathrm{T}} < 5.0\,\mathrm{GeV}/c$ were selected in the pseudorapidity range $|\eta| < 0.8$, in order to exclude non-uniformities due to the detector boundaries. Additional track quality cuts were applied to remove secondary particles (i.e. particles originating from weak decays, photon conversions and secondary hadronic interactions in the detector material) while maintaining good track reconstruction efficiency. Tracks were required to have at least 70 TPC space points out of the maximum of 159. The χ^2 of the track fit per degree of freedom in the TPC reconstruction was required to be below 2.

5 Systematic uncertainties

The evaluation of systematic uncertainties was performed by varying the event and track selection cuts and by studying the detector response with Monte Carlo (MC) simulations. For Pb–Pb, the track selection criteria were changed to only require tracks reconstructed in the TPC alone. This led to a significant difference in most of the observables (up to 10 %), which was taken into account in the estimation of the systematic uncertainties. Altering the number of TPC space points from 70 to 80, 90 and 100 resulted in a maximum 0.5% variation of v_n results. The variation of the v_n results when using other detectors, e.g. the SPD or TPC, to determine the centrality, is less than 0.5%. No significant variation of the v_n results was seen when altering the polarity of the magnetic field of the ALICE detector, or when narrowing the nominal $|z_{\mathrm{vtx}}|$ range from 10 cm to $|z_{\mathrm{vtx}}| < 7$, 8, and 9 cm. The contribution from pileup events to the final systematic uncertainty was found to be negligible. Systematic uncertainties due to detector inefficiencies were investigated using HIJING [56] and AMPT [57] MC simulations. The calculations for a sample at the event generator level (i.e. without invoking either the detector geometry or the reconstruction algorithm) were compared with the results of the analysis of the output of the full reconstruction with a GEANT3 [58] detector model, in a procedure referred to as an MC closure test. A difference of up to 4% for v_n is observed, which is included in the final systematic uncertainty. Most of the systematic uncertainties described above cancelled out for $v_n\{2\}/v_n[2]$ and r_n as indicated in table 2.

For p–Pb collisions, the approach used to evaluate the systematic uncertainty is similar. Different track quality cuts are applied, including varying the number of TPC space points, and using tracks reconstructed with the required TPC detector only instead of combined information from TPC and ITS. This leads to a systematic uncertainty of up to

JHEP09(2017)032

Pb–Pb sources	$v_2\{2\}$	$v_2[2]$	$v_3\{2\}$	$v_3[2]$	$v_4\{2\}$	$v_4[2]$
Track type	$< 4\%$	$< 4\%$	$< 10\%$	$< 8\%$	$< 8\%$	$< 8\%$
MC closure	$< 4\%$	$< 4\%$	$< 4\%$	$< 4\%$	$< 4\%$	$< 4\%$
Total	$< 5.7\%$	$< 5.7\%$	$< 10.7\%$	$< 9\%$	$< 9\%$	$< 9\%$

Table 1. Summary of systematic uncertainties of v_n for Pb–Pb collisions.

Pb–Pb sources	$v_2\{2\}/v_2[2]$	$v_3\{2\}/v_3[2]$	$v_4\{2\}/v_4[2]$	r_2	r_3
Track type	—	—	—	$< 2\%$	$< 5\%$
MC closure	$< 1\%$	$< 1\%$	$< 1\%$	$< 1\%$	$< 1\%$
Total	$< 1\%$	$< 1\%$	$< 1\%$	$< 2.2\%$	$< 5.1\%$

Table 2. Summary of systematic uncertainties of $v_n\{2\}/v_n[2]$ and r_n for Pb–Pb collisions.

p–Pb sources	$v_2\{2\}$	$v_2[2]$	$v_3\{2\}$	$v_3[2]$	$v_2\{2\}/v_2[2]$	r_2
Track type	$< 6\%$	$< 1\%$	—	—	$< 1\%$	$< 1\%$
MC closure	$< 9\%$	$< 8\%$	$< 3\%$	$< 2\%$	—	$< 1\%$
Total	$< 10.8\%$	$< 8.1\%$	$< 3\%$	$< 2\%$	$< 1\%$	$< 1.4\%$

Table 3. Summary of systematic uncertainties for p–Pb collisions.

6% depending on the multiplicity and p_{T} range. It was also found that varying the event selection, which includes the cut on the $|z_{\mathrm{vtx}}|$, and the cuts to reject pileup events, yields negligible contributions to the final systematic uncertainty. The analysis was repeated using the energy deposited in the neutron ZDC (ZNA) which is located at 112.5 m from the interaction point, instead of using V0-A for the event classes determination. The observed differences with respect to the one using V0-A for event class determination is not included as systematic uncertainty, following the previous paper [36]. In addition, the MC closure is investigated with DPMJET simulations [59] combined with GEANT3; this leads to a systematic uncertainty of less than 9% for $p_{\mathrm{T}} < 0.8\,\mathrm{GeV}/c$ and 2% for higher p_{T}.

The dominant sources of systematic uncertainty are summarized in tables 1, 2 and 3. The systematic uncertainties evaluated for each of the sources mentioned above were added in quadrature to obtain the total systematic uncertainty of the measurements.

6 Results and discussion

6.1 Pb–Pb collisions

Figures 1 and 2 show the p_{T} dependence of $v_2\{2\}$ and $v_2[2]$ with three different pseudorapidity gaps, for centrality classes from 0–5% to 70–80%. The analysed events are divided into two sub-events A and B, separated by a pseudorapidity gap. Note that $|\Delta\eta| > 0$ suggests that there is no separation in pseudorapidity between the two sub-events. Short-range correlations, one of the main sources of non-flow effects, are expected to be suppressed

JHEP09(2017)032

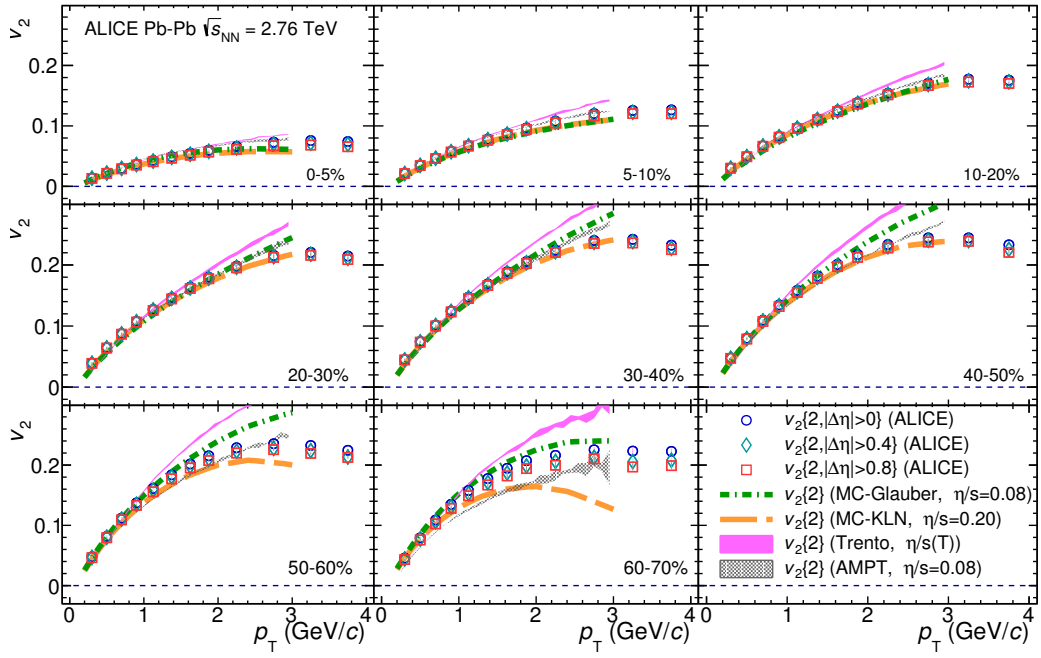


Figure 1. $v_2\{2\}$ with $|\Delta\eta| > 0$ (circles), $|\Delta\eta| > 0.4$ (diamonds) and $|\Delta\eta| > 0.8$ (squares) for various centrality classes in Pb–Pb collisions at $\sqrt{s_{\rm NN}} = 2.76$ TeV. Hydrodynamic calculations with MC-Glauber initial conditions and $\eta/s = 0.08$ [33], with MC-KLN initial conditions and $\eta/s = 0.20$ [33], with Trento initial conditions and temperature dependent η/s [60] and AMPT initial conditions and $\eta/s = 0.08$ [60] are shown in green dot-dash, orange dashed curves, and magenta and grey shaded areas, respectively.

when using a large pseudorapidity gap. It is observed that $v_2\{2\}$ and $v_2[2]$ using various pseudorapidity gaps do not change significantly for central and semi-central collisions. The decrease of v_2 with larger pseudorapidity gaps is more prominent in the most peripheral collisions, mainly due to the suppression of non-flow effects. The results are also compared to the original predictions within the `VISH2+1` hydrodynamic framework with: 1) Monte Carlo Glauber (MC-Glauber) initial conditions and $\eta/s = 0.08$; 2) Monte Carlo Kharzeev-Levin-Nardi (MC-KLN) initial conditions and $\eta/s = 0.20$ [33]. In addition, the comparisons to recently released calculations from the `iEBE-VISHNU` hydrodynamic framework with: 1) Trento initial conditions, temperature dependent shear and bulk viscosities, η/s(T) and ζ(T); and 2) AMPT initial conditions with $\eta/s = 0.08$ [60] are also presented. These combinations of various initial conditions and η/s are chosen due to the fact that they give the best descriptions of the particle spectra and the integrated flow measurements [60, 61]. The four hydrodynamic calculations describe the $v_2\{2\}$ very well up to $p_{\rm T} \approx 2\,{\rm GeV}/c$ at least for central and semi-central collisions, as do the calculations with MC-Glauber, MC-KLN and AMPT initial conditions for the $v_2[2]$. For central and mid-central collisions, calculations with MC-KLN and AMPT initial conditions predict both $v_2\{2\}$ and $v_2[2]$ better for higher $p_{\rm T}$ than those with MC-Glauber and Trento initial conditions. For more peripheral collisions, the experimental v_2 data in both cases fall between the four sets of predictions.

In order to probe the $p_{\rm T}$-dependent flow vector fluctuations quantitatively, the ratio $v_2\{2, |\Delta\eta| > 0.8\}/v_2[2, |\Delta\eta| > 0.8]$ using eq. (2.3) is presented as a function of $p_{\rm T}$ for

JHEP09(2017)032

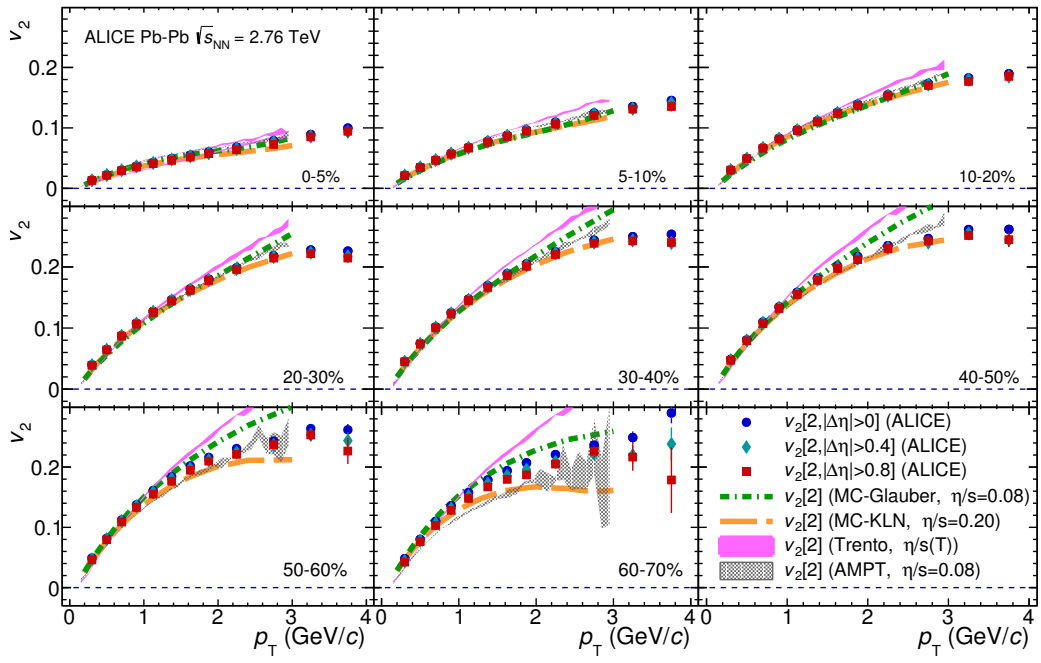


Figure 2. $v_2[2]$ with $|\Delta\eta| > 0$ (circles), $|\Delta\eta| > 0.4$ (diamonds) and $|\Delta\eta| > 0.8$ (squares) for various centrality classes in Pb–Pb collisions at $\sqrt{s_{\rm NN}} = 2.76\,\text{TeV}$. Hydrodynamic calculations with MC-Glauber initial conditions [33] and $\eta/s = 0.08$, with MC-KLN initial conditions and $\eta/s = 0.20$ [33], with Trento initial conditions and temperature dependent η/s [60] and AMPT initial conditions and $\eta/s = 0.08$ [60] are shown in green dot-dashed and orange dashed curves, and magenta and grey shaded areas, respectively.

different centrality classes in figure 3. This ratio is consistent with unity up to $p_{\rm T} \approx 2\,\text{GeV}/c$ and starts to deviate from unity in the higher $p_{\rm T}$ region in the most central collisions. The deviations from unity are weak and within 10% in non-central collisions in the presented $p_{\rm T}$ range. To better understand whether such deviations from unity are caused by non-flow effects, the like-sign technique, which suppresses contributions from resonance decays by correlating only particles with same charge, is applied. The differences of the measured $v_2\{2, |\Delta\eta| > 0.8\}/v_2[2, |\Delta\eta| > 0.8]$ from like-sign and all charged particles are found to be less than 0.5%. This shows that deviations of $v_2\{2, |\Delta\eta| > 0.8\}/v_2[2, |\Delta\eta| > 0.8]$ from unity cannot be explained solely by non-flow effects from resonance decays. It is also seen in figure 3 that the hydrodynamic calculations with MC-KLN, Trento and AMPT initial conditions describe the data fairly well for all centrality classes except for the most peripheral collisions, while MC-Glauber calculations reproduce the data only for mid-central and peripheral collisions. This indicates that hydrodynamic calculations with AMPT and MC-KLN initial conditions and $\eta/s = 0.20$ not only generate reasonable v_2 values, but also reproduce the measured $v_2\{2, |\Delta\eta| > 0.8\}/v_2[2, |\Delta\eta| > 0.8]$.

The higher order anisotropic flow coefficients, which were first measured in [20], are shown to be more sensitive to the initial conditions and η/s [12]. In figures 4 and 5, $v_3\{2\}$ and $v_3[2]$ are shown with three different pseudorapidity gaps for several centrality classes. Similar to what was presented in figures 1 and 2, both $v_3\{2\}$ and $v_3[2]$ show a decreasing

JHEP09(2017)032

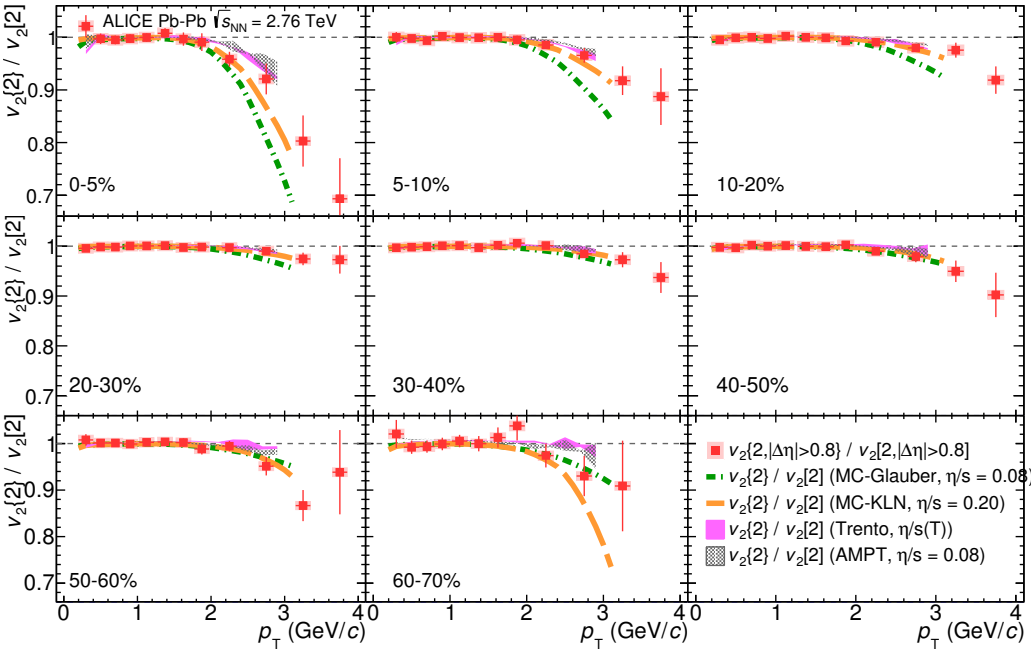


Figure 3. The ratio $v_2\{2, |\Delta\eta| > 0.8\}/v_2[2, |\Delta\eta| > 0.8]$ in Pb–Pb collisions at $\sqrt{s_{\rm NN}} = 2.76$ TeV. The different panels show the centrality evolution of the measurements. Hydrodynamic calculations with MC-Glauber initial conditions and $\eta/s = 0.08$ [33], with MC-KLN initial conditions and $\eta/s = 0.20$ [33], with Trento initial conditions and temperature dependent η/s [60] and AMPT initial conditions and $\eta/s = 0.08$ [60] are shown in green dot-dashed and orange dashed curves, and magenta and grey shaded areas, respectively.

trend as the pseudorapidity gap increases, in particular in more peripheral collisions. Only a weak centrality dependence is observed for both $v_3\{2\}$ and $v_3[2]$. The comparison to hydrodynamic calculations demonstrates that although hydrodynamic calculations with MC-Glauber and MC-KLN initial conditions roughly describe $v_2\{2\}$ and $v_2[2]$, they cannot describe $v_3\{2\}$ and $v_3[2]$ over the full $p_{\rm T}$ range and for all centrality classes, and tend to overpredict or underpredict the data. Similar as v_2, the hydrodynamic calculation with Trento initial conditions overestimates both $v_3\{2\}$ and $v_3[2]$ measurements, while the one with AMPT initial conditions quantitatively describe the measured v_3 for presented $p_{\rm T}$ and centrality intervals.

The ratio $v_3\{2, |\Delta\eta| > 0.8\}/v_3[2, |\Delta\eta| > 0.8]$ is shown together with hydrodynamic calculations in figure 6. Wider $p_{\rm T}$ intervals were used for the ratio than for the individual v_3 measurements in order to suppress statistical fluctuations. It was found that the ratio agrees with unity over a wide $p_{\rm T}$ range, as opposed to $v_2\{2, |\Delta\eta| > 0.8\}/v_2[2, |\Delta\eta| > 0.8]$. No clear indication of $p_{\rm T}$-dependent V_3 flow vector fluctuations are observed for the presented centrality and $p_{\rm T}$ regions within the large uncertainties. Despite the fact that the hydrodynamic calculations with MC-Glauber and MC-KLN initial conditions cannot reproduce the magnitude of $v_3\{2\}$ and $v_3[2]$, the validity of the two sets of initial conditions could be examined also by the comparison of the predicted $v_3\{2\}/v_3[2]$ ratio to data, which should be independent of the magnitude of v_3. Hydrodynamic calculations from `VISH2+1`,

JHEP09(2017)032

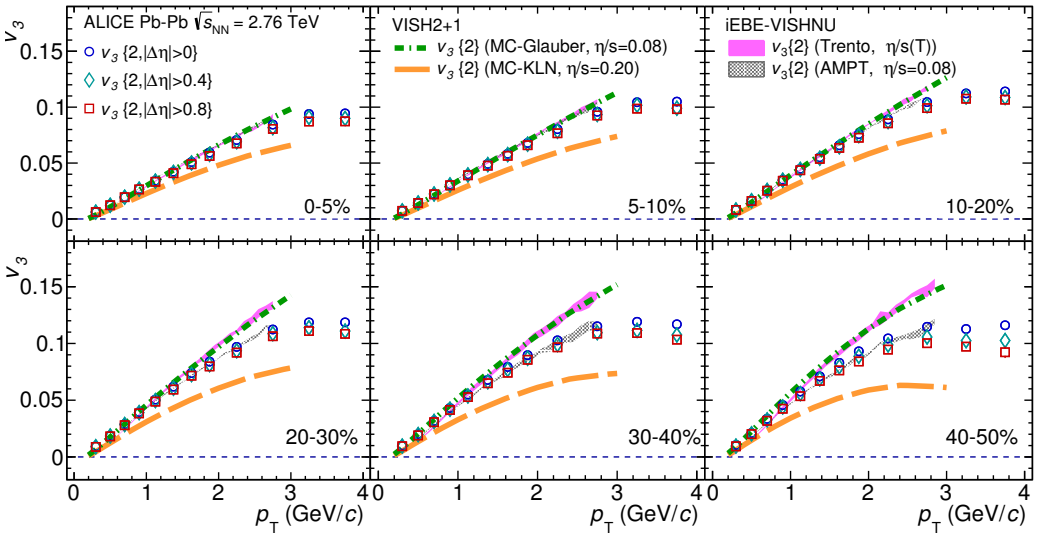


Figure 4. $v_3\{2\}$ with different $|\Delta\eta|$ gaps is presented in Pb–Pb collisions at $\sqrt{s_{\rm NN}} = 2.76\,\text{TeV}$. $v_3\{2, |\Delta\eta| > 0\}$, $v_3\{2, |\Delta\eta| > 0.4\}$, and $v_3\{2, |\Delta\eta| > 0.8\}$ are represented by circles, diamonds and squares, respectively. The different panels show the centrality evolution of the measurements. Hydrodynamic calculations with MC-Glauber initial conditions and $\eta/s = 0.08$ [33], with MC-KLN initial conditions and $\eta/s = 0.20$ [33], with Trento initial conditions and temperature dependent η/s [60] and AMPT initial conditions and $\eta/s = 0.08$ [60] are shown in green dot-dash, orange dashed curves, and magenta and grey shaded areas, respectively.

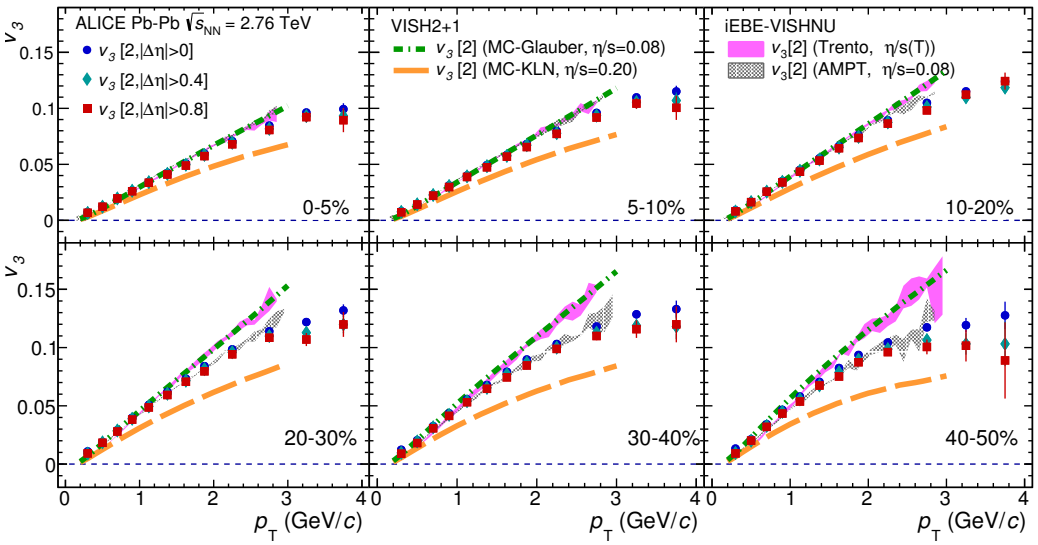


Figure 5. $v_3[2]$ with different $|\Delta\eta|$ gaps is presented in Pb–Pb collisions at $\sqrt{s_{\rm NN}} = 2.76\,\text{TeV}$. $v_3[2, |\Delta\eta| > 0]$, $v_3[2, |\Delta\eta| > 0.4]$, and $v_3[2, |\Delta\eta| > 0.8]$ are represented by circles, diamonds, and squares, respectively. The different panels show the centrality evolution of the measurements. Hydrodynamic calculations with MC-Glauber initial conditions and $\eta/s = 0.08$ [33] and with MC-KLN initial conditions and $\eta/s = 0.20$ [33], with Trento initial conditions and temperature dependent η/s [60] and AMPT initial conditions and $\eta/s = 0.08$ [60] are shown in green dot-dash, orange dashed curves, and magenta and grey shaded areas, respectively.

JHEP09(2017)032

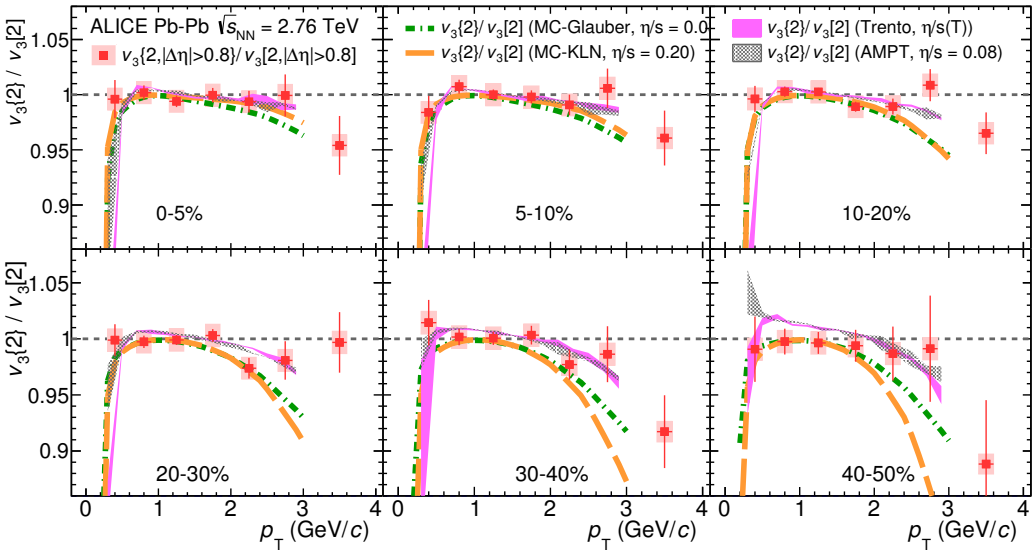


Figure 6. The ratio $v_3\{2, |\Delta\eta| > 0.8\}/v_3[2, |\Delta\eta| > 0.8]$ in Pb–Pb collisions at $\sqrt{s_{\rm NN}} = 2.76$ TeV. The different panels show the centrality evolution of the measurements. Hydrodynamic calculations with MC-Glauber initial conditions and $\eta/s = 0.08$ [33] and with MC-KLN initial conditions and $\eta/s = 0.20$ [33], with Trento initial conditions and temperature dependent η/s [60] and AMPT initial conditions and $\eta/s = 0.08$ [60] are shown in green dot-dash, orange dashed curves, and magenta and grey shaded areas, respectively.

especially the one with MC-KLN initial conditions, overestimate the possible $p_{\rm T}$-dependent V_3 flow vector fluctuations, despite the good description for the second harmonic. A good agreement between data and hydrodynamic calculations from `iEBE-VISHNU` is found for all centrality intervals. This is expected for AMPT initial conditions as the calculations quantitatively reproduce both measured $v_3\{2\}$ and $v_3[2]$ as discussed above. However, the calculations with Trento initial conditions, which overestimate both $v_3\{2\}$ and $v_3[2]$, are consistent with the measured $v_3\{2, |\Delta\eta| > 0.8\}/v_3[2, |\Delta\eta| > 0.8]$ ratio. This accidental agreement needs further investigations in the `iEBE-VISHNU` framework to understand the physics mechanism responsible for this behaviour.

The centrality dependence of $v_4\{2\}$ and $v_4[2]$ with three different pseudorapidity gaps are shown in figures 7 and 8. Decreasing trends with increasing $|\Delta\eta|$ gaps and a weak centrality dependence are observed for both measurements. The hydrodynamic calculations with MC-Glauber and Trento initial conditions overestimate the measurements of $v_4\{2\}$ and $v_4[2]$, while the calculations with MC-KLN initial conditions underestimate the measurements, similar to what was seen for the v_3 observables. On the other hand, the hydrodynamic calculations from AMPT initial conditions agree with the measurements of $v_4\{2\}$ and $v_4[2]$. Moreover, the ratio $v_4\{2, |\Delta\eta| > 0.8\}/v_4[2, |\Delta\eta| > 0.8]$ shown in figure 9 is in agreement with unity albeit with large uncertainties for the presented $p_{\rm T}$ range and centrality classes. The validity of the hydrodynamic calculations cannot be judged due to the large uncertainties of the $v_4\{2, |\Delta\eta| > 0.8\}/v_4[2, |\Delta\eta| > 0.8]$ measurements.

Alternatively, one can search for $p_{\rm T}$-dependent flow vector fluctuations via the measurement of the factorisation ratio, r_n. The results of r_2 and r_3 are presented in figures 10

JHEP09(2017)032

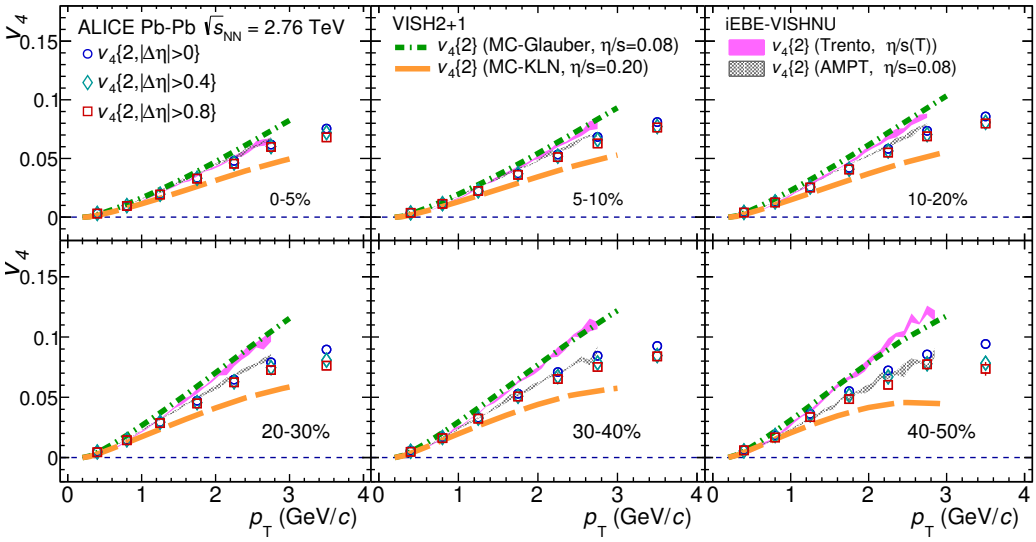


Figure 7. $v_4\{2\}$ with different $|\Delta\eta|$ gaps is presented in Pb–Pb collisions at $\sqrt{s_{\rm NN}} = 2.76\,\text{TeV}$. $v_4\{2, |\Delta\eta| > 0\}$, $v_4\{2, |\Delta\eta| > 0.4\}$ and $v_4\{2, |\Delta\eta| > 0.8\}$ are represented by circles, diamonds, and squares, respectively. The different panels show the centrality evolution of the measurements. Hydrodynamic calculations with MC-Glauber initial conditions and $\eta/s = 0.08$ [33], with MC-KLN initial conditions and $\eta/s = 0.20$ [33], with Trento initial conditions and temperature dependent η/s [60] and AMPT initial conditions and $\eta/s = 0.08$ [60] are shown in green dot-dash, orange dashed curves, and magenta and grey shaded areas, respectively.

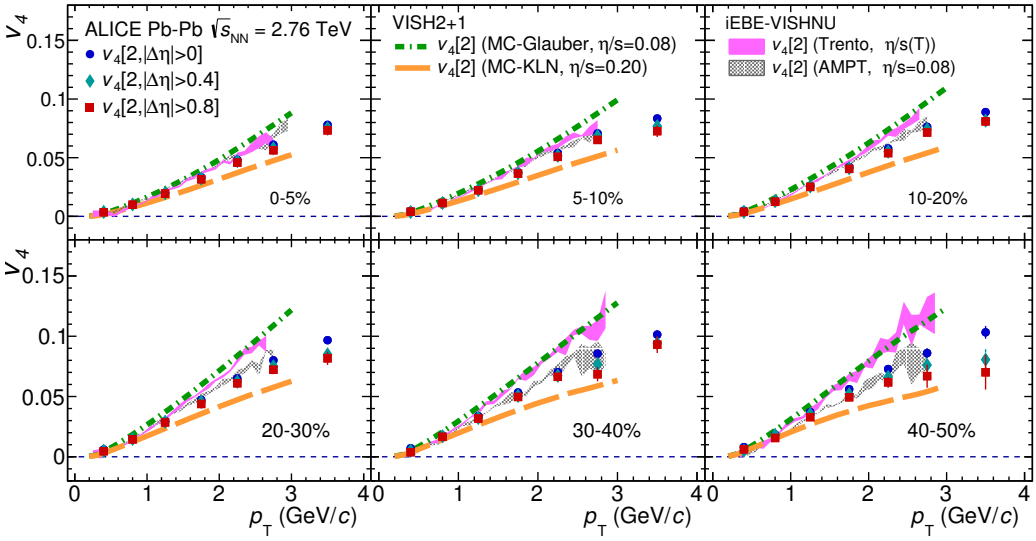


Figure 8. $v_4[2]$ with different $|\Delta\eta|$ gaps is presented in Pb–Pb collisions at $\sqrt{s_{\rm NN}} = 2.76\,\text{TeV}$. $v_4[2, |\Delta\eta| > 0]$, $v_4[2, |\Delta\eta| > 0.4]$, and $v_4[2, |\Delta\eta| > 0.8]$ are represented by circles, diamonds, and squares, respectively. The different panels show the centrality evolution of the measurements. Hydrodynamic calculations with MC-Glauber initial conditions and $\eta/s = 0.08$ [33] and with MC-KLN initial conditions and $\eta/s = 0.20$ [33], with Trento initial conditions and temperature dependent η/s [60] and AMPT initial conditions and $\eta/s = 0.08$ [60] are shown in green dot-dash, orange dashed curves, and magenta and grey shaded areas, respectively.

JHEP09(2017)032

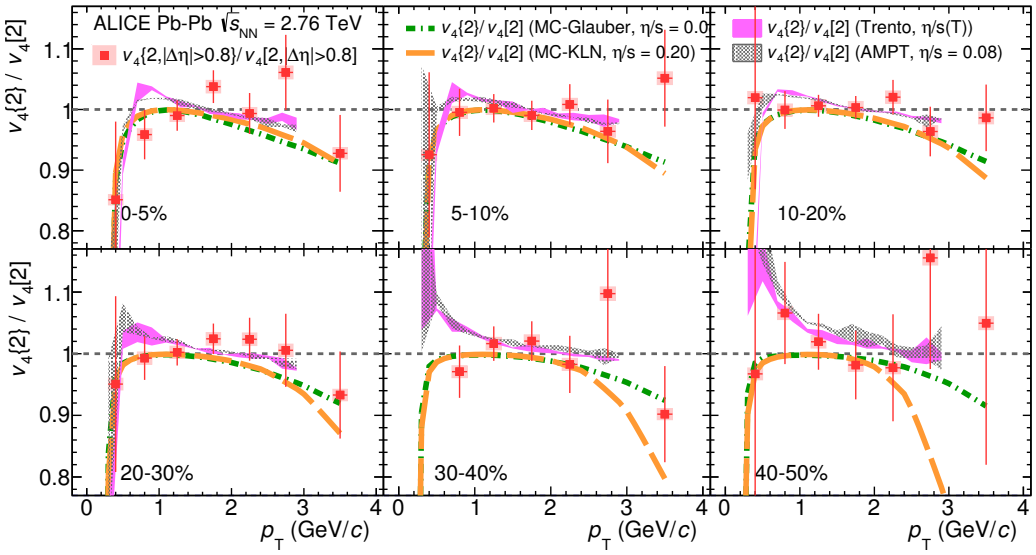


Figure 9. The ratio $v_4\{2, |\Delta\eta| > 0.8\}/v_4[2, |\Delta\eta| > 0.8]$ in Pb–Pb collisions at $\sqrt{s_{\rm NN}} = 2.76\,\text{TeV}$. The different panels show the centrality evolution of the measurements. Hydrodynamic calculations with MC-Glauber initial conditions and $\eta/s = 0.08$ [33] and with MC-KLN initial conditions and $\eta/s = 0.20$ [33], with Trento initial conditions and temperature dependent η/s [60] and AMPT initial conditions and $\eta/s = 0.08$ [60] are shown in green dot-dash, orange dashed curves, and magenta and grey shaded areas, respectively.

and 11 as a function of $p_{\rm T}^t$ and $p_{\rm T}^a$ with $|\Delta\eta| > 0.8$ for three centrality classes in Pb–Pb collisions at $\sqrt{s_{\rm NN}} = 2.76\,\text{TeV}$. By construction, $r_n = 1$ when the triggered and associated particles are from the same $p_{\rm T}$ interval. In contrast to the previous analysis [34], there is no $p_{\rm T}^t \geq p_{\rm T}^a$ cut applied here to avoid auto-correlations (taking the same particle as both triggered and associated particles in the two-particle azimuthal correlations). The triggered particles are always selected from the negative pseudorapidity region and the associated particles are from the positive pseudorapidity region. The r_2 value deviates significantly from unity for the most central collisions. This effect becomes stronger with an increasing difference between $p_{\rm T}^t$ and $p_{\rm T}^a$. The previous results indicated that factorisation holds approximately for $n \geq 2$ and $p_{\rm T}$ below $4\,\text{GeV}/c$, while deviations emerging at higher $p_{\rm T}$ were ascribed to recoil jet contributions [34]. This analysis, however, shows that factorisation breaks down at lower $p_{\rm T}$ when the more sensitive observable, r_2, is used. The deviation reaches 10% for the lowest $p_{\rm T}^a$ in the 0–5% centrality range, for $2.5 < p_{\rm T}^t < 3\,\text{GeV}/c$. One explanation from [32] is that this deviation is due to the $p_{\rm T}$-dependent V_2 flow vector fluctuations, which originate from initial event-by-event geometry fluctuations. Hydrodynamic calculations [33] are compared to data for the presented centrality classes and for selected $p_{\rm T}$ bins. Both hydrodynamic calculations from `VISH2+1` and `iEBE-VISHNU` frameworks qualitatively predict the trend of r_2, while the data agree quantitatively better with `iEBE-VISHNU`. In addition, the CMS measurements [41, 47] are consistent with our measurements.

For r_3, the results are compatible with unity, and can be described by hydrodynamic calculations from both `VISH2+1` and `iEBE-VISHNU` frameworks, albeit with large statistical

JHEP09(2017)032

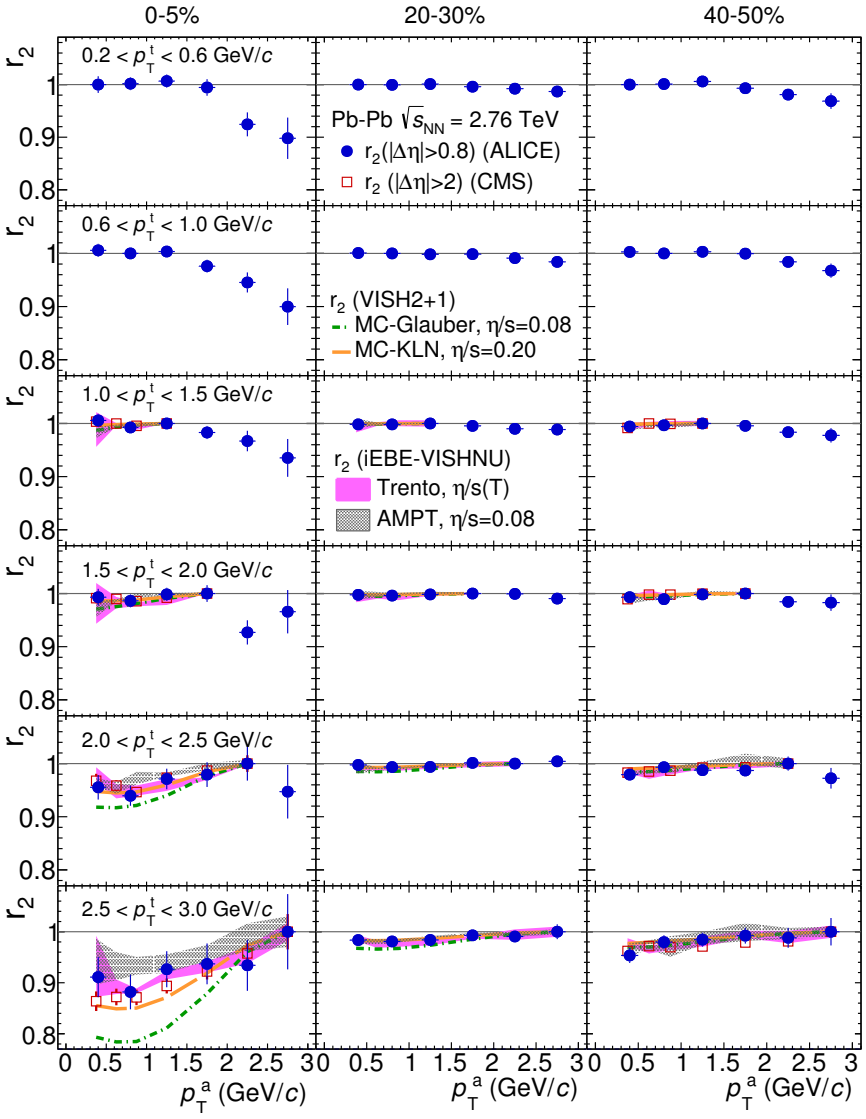


Figure 10. The factorisation ratio r_2, as a function of p_{T}^a in bins of p_{T}^t for 0–5%, 20–30% and 40–50% centralities in Pb–Pb collisions at $\sqrt{s_{\mathrm{NN}}} = 2.76\,\mathrm{TeV}$, is presented (solid circles). CMS measurements are presented by open square [41]. Hydrodynamic calculations with MC-Glauber initial conditions and $\eta/s = 0.08$ [33] and with MC-KLN initial conditions and $\eta/s = 0.20$ [33], with Trento initial conditions and temperature dependent η/s [60] and AMPT initial conditions and $\eta/s = 0.08$ [60] are shown in green dot-dash, orange dashed curves, and magenta and grey shaded areas, respectively.

uncertainties. The factorisation is valid over a wider range of p_{T}^a, p_{T}^t and centrality ranges, as opposed to r_2. The possible breakdown of factorisation, if it exists, is within 10% when both p_{T}^a and p_{T}^t are below $3\,\mathrm{GeV}/c$. The CMS measurements [41, 47] are consistent with the r_3 results presented here despite the fact that the pseudorapidity gaps are different between the two measurements. Better agreements with hydrodynamic calculations are observed with `VISH2+1`.

JHEP09(2017)032

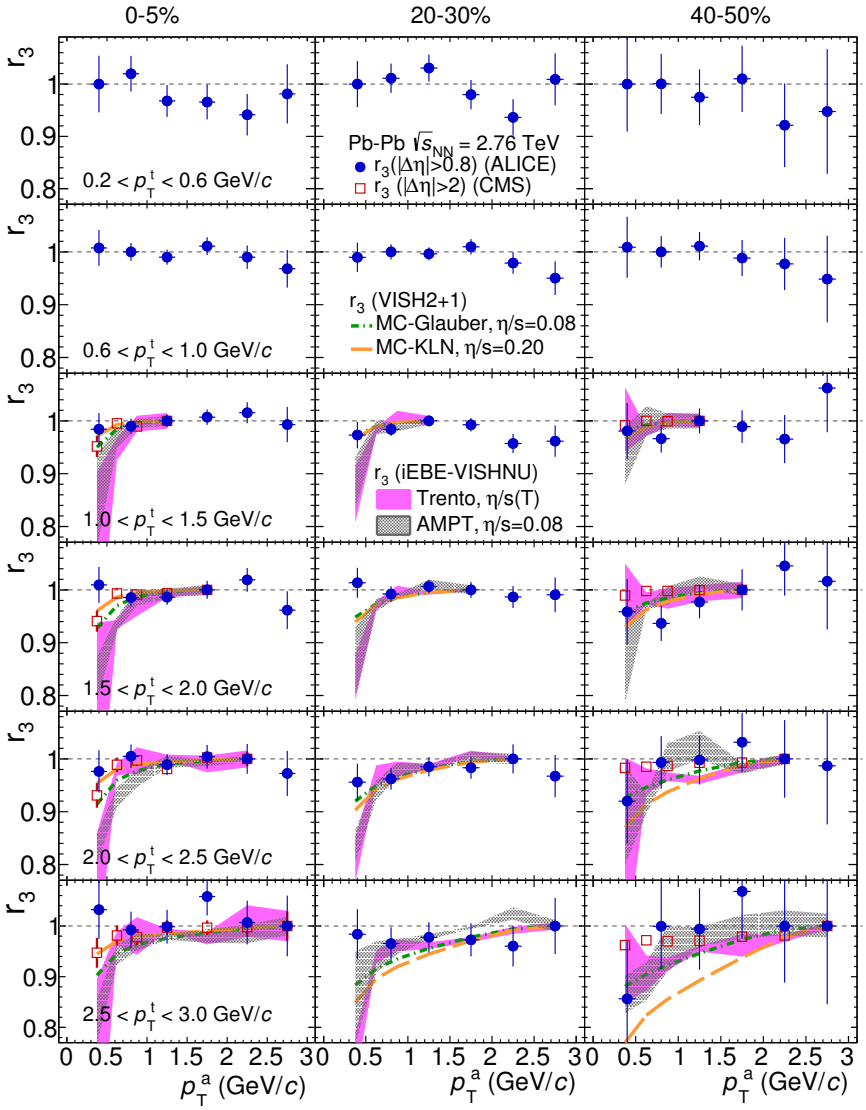


Figure 11. The factorisation ratio r_3, as a function of p_{T}^{a} in bins of p_{T}^{t} for 0–5%, 20–30% and 40–50% centralities in Pb–Pb collisions at $\sqrt{s_{\mathrm{NN}}} = 2.76\,\mathrm{TeV}$, is presented (solid circles). CMS measurements [41] are presented by open squares. Hydrodynamic calculations with MC-Glauber initial conditions and $\eta/s = 0.08$ [33] and with MC-KLN initial conditions and $\eta/s = 0.20$ [33], with Trento initial conditions and temperature dependent η/s [60] and AMPT initial conditions and $\eta/s = 0.08$ [60] are shown in green dot-dash, orange dashed curves, and magenta and grey shaded areas, respectively.

6.2 p–Pb collisions

Figure 12 presents $v_2\{2\}$ and $v_2[2]$ with $|\Delta\eta| > 0$ and $|\Delta\eta| > 0.8$ for various multiplicity classes in p–Pb collisions at $\sqrt{s_{\mathrm{NN}}} = 5.02\,\mathrm{TeV}$. It is shown that, after applying the pseudorapidity gap $|\Delta\eta| > 0.8$, both $v_2\{2\}$ and $v_2[2]$ decrease substantially, in particular for more peripheral collisions, mainly due to the reduction of non-flow effects. The ratio $v_2\{2, |\Delta\eta| > 0.8\}/v_2[2, |\Delta\eta| > 0.8]$, shown in figure 13, displays hints of deviations from

JHEP09(2017)032

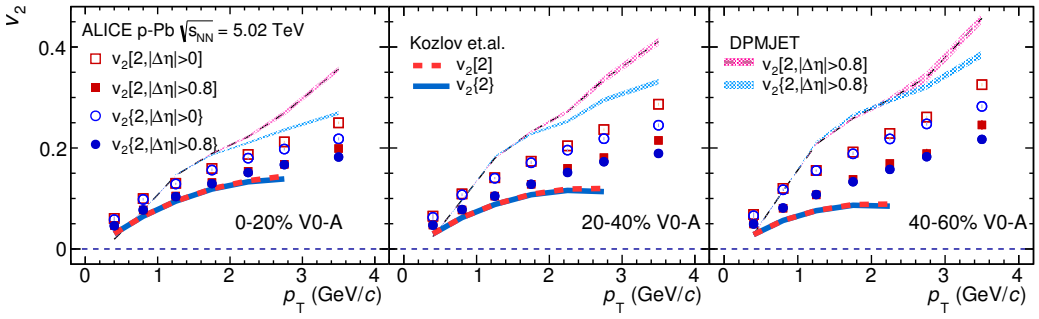


Figure 12. $v_2\{2, |\Delta\eta| > 0\}$, $v_2[2, |\Delta\eta| > 0]$, $v_2\{2, |\Delta\eta| > 0.8\}$ and $v_2[2, |\Delta\eta| > 0.8]$ for various multiplicity classes of p–Pb collisions at $\sqrt{s_{\rm NN}} = 5.02\,\text{TeV}$. DPMJET calculations are presented by red shaded lines for $v_2\{2, |\Delta\eta| > 0.8\}$ and blue shaded lines for $v_2[2, |\Delta\eta| > 0.8]$. Hydrodynamic calculations (MUSIC) [62] with modified MC-Glauber initial conditions and $\eta/s = 0.08$ for $v_2\{2\}$ and $v_2[2]$ are shown in solid blue and dashed red lines.

unity above $p_{\rm T} \approx 2\,\text{GeV}/c$, but the statistical uncertainties are still too large to draw a firm conclusion. The DPMJET model [59], which is an implementation of the two-component Dual Parton Model for the description of interactions involving nuclei, and contains no collective effects, has been used as a benchmark to study the influence of non-flow in p–Pb collisions [38]. The calculations based on DPMJET simulations are compared to data. It is observed in figure 12 that DPMJET overestimates v_2 significantly for the presented multiplicity classes, and generates higher v_2 coefficients in lower multiplicity regions. Meanwhile, figure 13 shows that for $v_2\{2\}/v_2[2]$ the agreement between data and DPMJET is better in low multiplicity p–Pb collisions, where no evidence of anisotropic collectivity is achieved from previous measurements [36, 38]. In addition, the hydrodynamic calculations [62] from MUSIC v2.0 using a modified MC-Glauber initial state and $\eta/s = 0.08$ are also presented in figures 12 and 13. These calculations in general underpredict the measured v_2 coefficients but agree better with the data in high multiplicity than in low multiplicity classes. It should be emphasized that in contrast to hydrodynamic calculations, the measured $v_2\{2\}$ and $v_2[2]$ increase (albeit very slightly in particular when the $|\Delta\eta|$ gap is applied) from 0–20% to 40–60% multiplicity classes, which indicates that non-flow effects might play a more important role in low multiplicity events. This could explain the increasing deviation between data and hydrodynamic calculations with $p_{\rm T}$ and towards lower multiplicity classes, shown in figure 12. The hydrodynamic calculations reproduce the $v_2\{2\}/v_2[2]$ measurements in the 0–20 % multiplicity class, which seems to indicate that hydrodynamic collectivity is present in high multiplicity p–Pb collisions. However, it is still unclear at the moment why the measured ratio is still reproduced by hydrodynamic calculations for multiplicity class above 20%, where no significant flow signal is expected to be produced [38]. The agreement might be accidental since the DPMJET and hydrodynamic calculations also agree with each other in this class.

The $v_3\{2\}$ and $v_3[2]$ measured with $|\Delta\eta| > 0$ and $|\Delta\eta| > 0.8$ in p–Pb collisions at $\sqrt{s_{\rm NN}} = 5.02\,\text{TeV}$ are shown in figure 14. Both $v_3\{2, |\Delta\eta| > 0\}$ and $v_3[2, |\Delta\eta| > 0]$ increase with $p_{\rm T}$ and also with decreasing multiplicity. The measured $v_3\{2\}$ and $v_3[2]$ with a pseudorapidity gap of $|\Delta\eta| > 0.8$ are much smaller than those with $|\Delta\eta| > 0$, with the

JHEP09(2017)032

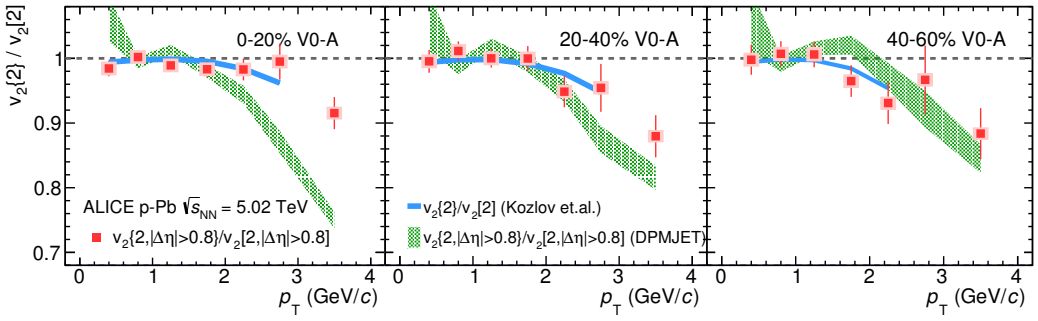


Figure 13. The ratio $v_2\{2, |\Delta\eta| > 0.8\}/v_2[2, |\Delta\eta| > 0.8]$ for various multiplicity classes in p–Pb collisions at $\sqrt{s_{\rm NN}} = 5.02\,\text{TeV}$. DPMJET calculations are presented by green shaded lines. Hydrodynamic calculations (MUSIC) [62] with modified MC-Glauber initial conditions and $\eta/s = 0.08$ are shown as solid blue lines.

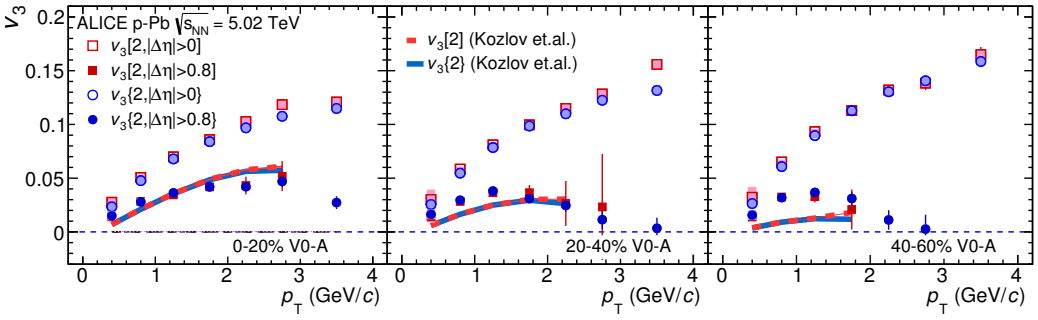


Figure 14. $v_3\{2, |\Delta\eta| > 0\}$, $v_3[2, |\Delta\eta| > 0]$, $v_3\{2, |\Delta\eta| > 0.8\}$ and $v_3[2, |\Delta\eta| > 0.8]$ for various multiplicity classes in p–Pb collisions at $\sqrt{s_{\rm NN}} = 5.02\,\text{TeV}$. Hydrodynamic calculations (MUSIC) [62] with modified MC-Glauber initial conditions and $\eta/s = 0.08$ for $v_2\{2\}$ and $v_2[2]$ are shown as solid blue and dashed red lines.

deviation increasing as a function of $p_{\rm T}$. The relative influence of non-flow effects appears to be stronger in v_3 than in v_2 measurements. A similar qualitative behaviour was observed for $p_{\rm T}$-integrated two-particle cumulants $c_2\{2\}$ and $c_3\{2\}$ in p–Pb collisions, measured as functions of multiplicity for different $|\Delta\eta|$ gaps [36]. It might be worth noting that part of the remaining non-flow contamination with $|\Delta\eta| > 0.8$, the recoil jet ridge, has a positive sign contribution for v_2 and a negative sign one for v_3 for $p_{\rm T} > 2\,\text{GeV}/c$. In addition, it is found that hydrodynamic calculations describe the data better at high multiplicity than at low multiplicity, while DPMJET generates negative $(v_3[2])^2$ values for all multiplicity classes and thus cannot be shown here for comparison. Furthermore, the deviations between $v_3\{2, |\Delta\eta| > 0.8\}$ and $v_3[2, |\Delta\eta| > 0.8]$ are not observed for the presented $p_{\rm T}$ region. There is no indication of $p_{\rm T}$-dependent V_3 flow vector fluctuations in p–Pb collisions.

Figure 15 shows $r_2(|\Delta\eta| > 0.8)$ measurements as a function of $p_{\rm T}^a$ in three $p_{\rm T}^t$ intervals for multiplicity classes 0–20%, 20–40% and 40–60% in p–Pb collisions at $\sqrt{s_{\rm NN}} = 5.02\,\text{TeV}$. The $r_2(|\Delta\eta| > 0.8)$ deviates from unity when the $p_{\rm T}^t$ and $p_{\rm T}^a$ are well away from each other (most pronouncedly in the lowest and highest $p_{\rm T}^t$ bins) with the trend being similar for all multiplicity classes. As mentioned earlier, the deviation is more significant at high multiplicity. In overlapping $p_{\rm T}^t$ and $p_{\rm T}^a$ intervals, the r_2 measurements in the highest

JHEP09(2017)032

multiplicity p–Pb events are consistent with those made by CMS collaboration [47]. The breakdown of factorisation is more pronounced in high multiplicity p–Pb collisions than in the 40–50% centrality class in Pb–Pb collisions (see figure 10). The DPMJET calculations are presented for comparison. It is clearly seen that DPMJET overestimates the deviations of r_2 from unity in the high multiplicity region, nevertheless, the calculation describes the data better in low multiplicity events in which non-flow effects are dominant. At the same time, these measurements are found to be compatible with hydrodynamic calculations using modified MC-Glauber initial conditions and $\eta/s = 0.08$. When selecting the triggered particles from $0.6 < p_{\mathrm{T}}^{t} < 1.0\,\mathrm{GeV}/c$ or $1.0 < p_{\mathrm{T}}^{t} < 1.5\,\mathrm{GeV}/c$, the trend of r_2 looks similar to that of $v_2\{2\}/v_2[2]$, mainly because the mean p_{T} of charged particles is within $0.6 < \langle p_{\mathrm{T}} \rangle < 1.0\,\mathrm{GeV}/c$ [63].

7 Summary

Searches for p_{T}-dependent flow vector fluctuations are performed by measuring $v_n\{2\}/v_n[2]$ and r_n in Pb–Pb collisions at $\sqrt{s_{\mathrm{NN}}} = 2.76\,\mathrm{TeV}$ and p–Pb collisions at $\sqrt{s_{\mathrm{NN}}} = 5.02\,\mathrm{TeV}$. In Pb–Pb collisions, both $v_2\{2\}/v_2[2]$ and r_2 show deviations from unity, and the r_2 results are consistent with previous measurements from the CMS collaboration. These effects are more pronounced in the most central collisions and cannot be explained solely by non-flow effects. Therefore, these results suggest the presence of possible V_2 vector fluctuations in Pb–Pb collisions. It further implies that the traditional $v_2\{2\}$ results should be interpreted precisely as the correlations of the azimuthal angle of produced particles with respect to the p_{T} integrated flow vector over a certain kinematic region. Future comparisons between theoretical calculations and experimental measurements should be based on the same kinematic conditions. These comparisons, performed under carefully defined precisely matching kinematic conditions, are crucial to constrain the initial conditions and precisely extract the transport properties of the produced matter, without possible bias from additional p_{T}-dependent flow vector fluctuations. Meanwhile, no significant deviation of $v_3\{2\}/v_3[2]$ or $v_4\{2\}/v_4[2]$ from unity was observed, meaning that there is no indication of p_{T}-dependent V_3 and V_4 vector fluctuations. The comparison to hydrodynamic calculations shows only the calculations from `iEBE-VISHNU` with AMPT initial conditions could describe the data quantitatively. The measurements presented in this paper provide a unique approach to constrain the initial conditions and transport properties, e.g. shear viscosity over entropy density ratio η/s of the QGP, complementing the previous anisotropic flow measurements. The results therefore bring new insights into the properties of the QGP produced in relativistic heavy ion collisions at the CERN Large Hadron Collider.

Similar studies were performed in various multiplicity classes in p–Pb collisions. Deviations of $v_2\{2\}/v_2[2]$ and r_2 from unity are observed, although with relatively large statistical fluctuations. For the highest p–Pb multiplicity class, the deviations are significantly overestimated by DPMJET; however, they are compatible with hydrodynamic calculations using modified MC-Glauber initial conditions and $\eta/s = 0.08$. Meanwhile for low multiplicity p–Pb collisions, the data sits between calculations from DPMJET and hydrodynamics. Neither the DPMJET model, which does not incorporate anisotropic flow,

JHEP09(2017)032

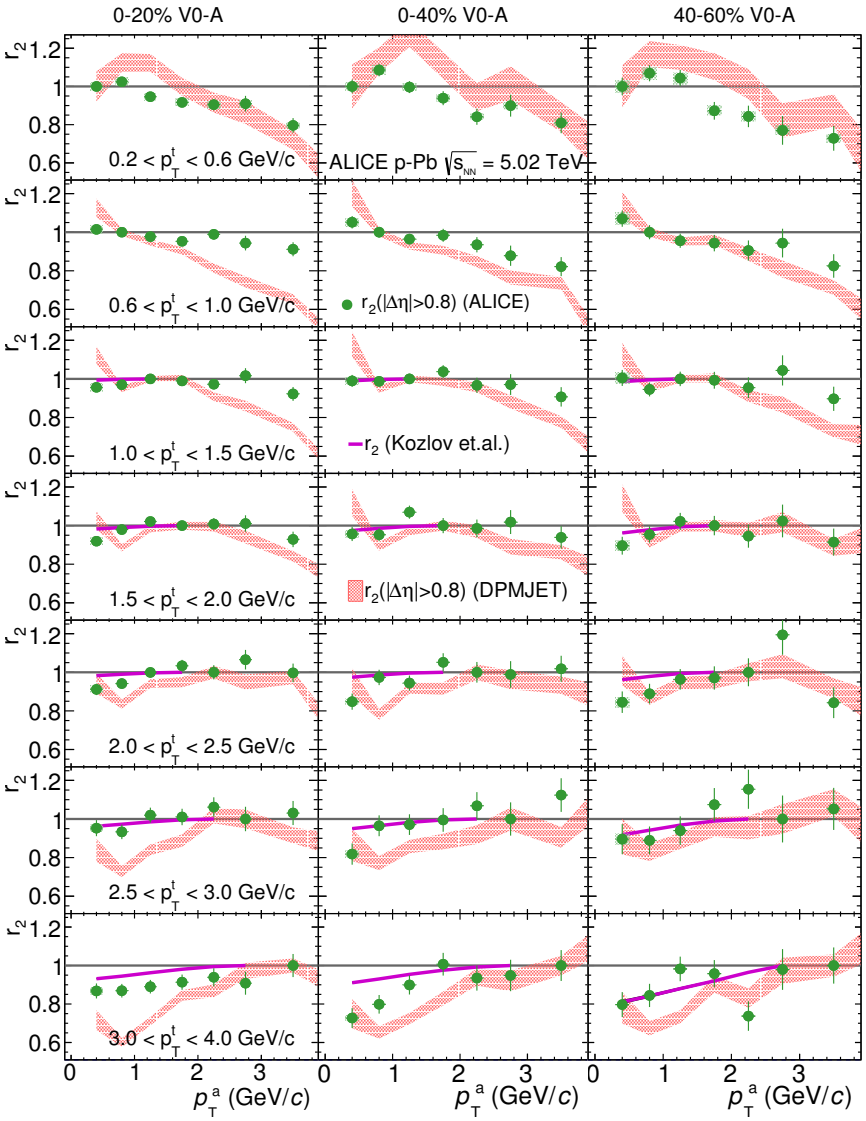


Figure 15. The factorisation ratio r_2, as a function of p_{T}^a in bins of p_{T}^t for multiplicity classes 0–20%, 20–40% and 40–60% in p–Pb collisions at $\sqrt{s_{\mathrm{NN}}} = 5.02\,\mathrm{TeV}$, are presented by solid magenta circles. DPMJET calculations are presented by pink shaded areas. Hydrodynamic calculations (MUSIC) with modified MC-Glauber initial conditions and $\eta/s = 0.08$ are shown as magenta lines [62].

nor the hydrodynamic model, which does not include non-flow contributions, could provide a quantitative description of the data. Future theoretical developments together with comparisons to high-precision measurements are crucial to give a certain answer concerning p_{T}-dependent vector V_n fluctuations in p–Pb collisions.

Acknowledgments

The ALICE collaboration would like to thank all its engineers and technicians for their invaluable contributions to the construction of the experiment and the CERN accelerator

JHEP09(2017)032

teams for the outstanding performance of the LHC complex. The ALICE collaboration gratefully acknowledges the resources and support provided by all Grid centres and the Worldwide LHC Computing Grid (WLCG) collaboration. The ALICE collaboration acknowledges the following funding agencies for their support in building and running the ALICE detector: A.I. Alikhanyan National Science Laboratory (Yerevan Physics Institute) Foundation (ANSL), State Committee of Science and World Federation of Scientists (WFS), Armenia; Austrian Academy of Sciences and Nationalstiftung für Forschung, Technologie und Entwicklung, Austria; Ministry of Communications and High Technologies, National Nuclear Research Center, Azerbaijan; Conselho Nacional de Desenvolvimento Científico e Tecnológico (CNPq), Universidade Federal do Rio Grande do Sul (UFRGS), Financiadora de Estudos e Projetos (Finep) and Fundação de Amparo à Pesquisa do Estado de São Paulo (FAPESP), Brazil; Ministry of Science & Technology of China (MSTC), National Natural Science Foundation of China (NSFC) and Ministry of Education of China (MOEC) , China; Ministry of Science, Education and Sport and Croatian Science Foundation, Croatia; Ministry of Education, Youth and Sports of the Czech Republic, Czech Republic; The Danish Council for Independent Research — Natural Sciences, the Carlsberg Foundation and Danish National Research Foundation (DNRF), Denmark; Helsinki Institute of Physics (HIP), Finland; Commissariat à l'Energie Atomique (CEA) and Institut National de Physique Nucléaire et de Physique des Particules (IN2P3) and Centre National de la Recherche Scientifique (CNRS), France; Bundesministerium für Bildung, Wissenschaft, Forschung und Technologie (BMBF) and GSI Helmholtzzentrum für Schwerionenforschung GmbH, Germany; General Secretariat for Research and Technology, Ministry of Education, Research and Religions, Greece; National Research, Development and Innovation Office, Hungary; Department of Atomic Energy Government of India (DAE) and Council of Scientific and Industrial Research (CSIR), New Delhi, India; Indonesian Institute of Science, Indonesia; Centro Fermi — Museo Storico della Fisica e Centro Studi e Ricerche Enrico Fermi and Istituto Nazionale di Fisica Nucleare (INFN), Italy; Institute for Innovative Science and Technology , Nagasaki Institute of Applied Science (IIST), Japan Society for the Promotion of Science (JSPS) KAKENHI and Japanese Ministry of Education, Culture, Sports, Science and Technology (MEXT), Japan; Consejo Nacional de Ciencia (CONACYT) y Tecnología, through Fondo de Cooperación Internacional en Ciencia y Tecnología (FONCICYT) and Dirección General de Asuntos del Personal Academico (DGAPA), Mexico; Nederlandse Organisatie voor Wetenschappelijk Onderzoek (NWO), Netherlands; The Research Council of Norway, Norway; Commission on Science and Technology for Sustainable Development in the South (COMSATS), Pakistan; Pontificia Universidad Católica del Perú, Peru; Ministry of Science and Higher Education and National Science Centre, Poland; Korea Institute of Science and Technology Information and National Research Foundation of Korea (NRF), Republic of Korea; Ministry of Education and Scientific Research, Institute of Atomic Physics and Romanian National Agency for Science, Technology and Innovation, Romania; Joint Institute for Nuclear Research (JINR), Ministry of Education and Science of the Russian Federation and National Research Centre Kurchatov Institute, Russia; Ministry of Education, Science, Research and Sport of the Slovak Republic, Slovakia; National Research Foundation of South Africa, South Africa; Centro de Aplicaciones

JHEP09(2017)032

Tecnológicas y Desarrollo Nuclear (CEADEN), Cubaenergía, Cuba, Ministerio de Ciencia e Innovacion and Centro de Investigaciones Energéticas, Medioambientales y Tecnológicas (CIEMAT), Spain; Swedish Research Council (VR) and Knut & Alice Wallenberg Foundation (KAW), Sweden; European Organization for Nuclear Research, Switzerland; National Science and Technology Development Agency (NSDTA), Suranaree University of Technology (SUT) and Office of the Higher Education Commission under NRU project of Thailand, Thailand; Turkish Atomic Energy Agency (TAEK), Turkey; National Academy of Sciences of Ukraine, Ukraine; Science and Technology Facilities Council (STFC), United Kingdom; National Science Foundation of the United States of America (NSF) and United States Department of Energy, Office of Nuclear Physics (DOE NP), United States of America.

Open Access. This article is distributed under the terms of the Creative Commons Attribution License (CC-BY 4.0), which permits any use, distribution and reproduction in any medium, provided the original author(s) and source are credited.

References

[1] E.V. Shuryak, *Quark-gluon Plasma and Hadronic Production of Leptons, Photons and Psions*, *Phys. Lett.* **B 78** (1978) 150 [INSPIRE].

[2] E.V. Shuryak, *Quantum Chromodynamics and the Theory of Superdense Matter*, *Phys. Rept.* **61** (1980) 71 [INSPIRE].

[3] J.-Y. Ollitrault, *Anisotropy as a signature of transverse collective flow*, *Phys. Rev.* **D 46** (1992) 229 [INSPIRE].

[4] S.A. Voloshin, A.M. Poskanzer and R. Snellings, *Collective phenomena in non-central nuclear collisions*, arXiv:0809.2949 [INSPIRE].

[5] U. Heinz and R. Snellings, *Collective flow and viscosity in relativistic heavy-ion collisions*, *Ann. Rev. Nucl. Part. Sci.* **63** (2013) 123 [arXiv:1301.2826] [INSPIRE].

[6] S. Voloshin and Y. Zhang, *Flow study in relativistic nuclear collisions by Fourier expansion of Azimuthal particle distributions*, *Z. Phys.* **C 70** (1996) 665 [hep-ph/9407282] [INSPIRE].

[7] A.M. Poskanzer and S.A. Voloshin, *Methods for analyzing anisotropic flow in relativistic nuclear collisions*, *Phys. Rev.* **C 58** (1998) 1671 [nucl-ex/9805001] [INSPIRE].

[8] A.P. Mishra, R.K. Mohapatra, P.S. Saumia and A.M. Srivastava, *Super-horizon fluctuations and acoustic oscillations in relativistic heavy-ion collisions*, *Phys. Rev.* **C 77** (2008) 064902 [arXiv:0711.1323] [INSPIRE].

[9] A.P. Mishra, R.K. Mohapatra, P.S. Saumia and A.M. Srivastava, *Using cosmic microwave background radiation analysis tools for flow anisotropies in relativistic heavy-ion collisions*, *Phys. Rev.* **C 81** (2010) 034903 [arXiv:0811.0292] [INSPIRE].

[10] J. Takahashi et al., *Topology studies of hydrodynamics using two particle correlation analysis*, *Phys. Rev. Lett.* **103** (2009) 242301 [arXiv:0902.4870] [INSPIRE].

[11] B. Alver and G. Roland, *Collision-geometry fluctuations and triangular flow in heavy-ion collisions*, *Phys. Rev.* **C 81** (2010) 054905 [*Erratum ibid.* **C 82** (2010) 039903] [arXiv:1003.0194] [INSPIRE].

[12] B.H. Alver, C. Gombeaud, M. Luzum and J.-Y. Ollitrault, *Triangular flow in hydrodynamics and transport theory*, *Phys. Rev.* **C 82** (2010) 034913 [arXiv:1007.5469] [INSPIRE].

JHEP09(2017)032

[13] D. Teaney and L. Yan, *Triangularity and Dipole Asymmetry in Heavy Ion Collisions*, *Phys. Rev.* **C 83** (2011) 064904 [arXiv:1010.1876] [INSPIRE].

[14] M. Luzum, *Collective flow and long-range correlations in relativistic heavy ion collisions*, *Phys. Lett.* **B 696** (2011) 499 [arXiv:1011.5773] [INSPIRE].

[15] BRAHMS collaboration, I. Arsene et al., *Quark gluon plasma and color glass condensate at RHIC? The Perspective from the BRAHMS experiment*, *Nucl. Phys.* **A 757** (2005) 1 [nucl-ex/0410020] [INSPIRE].

[16] PHOBOS collaboration, B.B. Back et al., *The PHOBOS perspective on discoveries at RHIC*, *Nucl. Phys.* **A 757** (2005) 28 [nucl-ex/0410022] [INSPIRE].

[17] STAR collaboration, J. Adams et al., *Experimental and theoretical challenges in the search for the quark gluon plasma: The STAR collaboration's critical assessment of the evidence from RHIC collisions*, *Nucl. Phys.* **A 757** (2005) 102 [nucl-ex/0501009] [INSPIRE].

[18] PHENIX collaboration, K. Adcox et al., *Formation of dense partonic matter in relativistic nucleus-nucleus collisions at RHIC: Experimental evaluation by the PHENIX collaboration*, *Nucl. Phys.* **A 757** (2005) 184 [nucl-ex/0410003] [INSPIRE].

[19] ALICE collaboration, *Elliptic flow of charged particles in Pb-Pb collisions at* 2.76 *TeV*, *Phys. Rev. Lett.* **105** (2010) 252302 [arXiv:1011.3914] [INSPIRE].

[20] ALICE collaboration, *Higher harmonic anisotropic flow measurements of charged particles in Pb-Pb collisions at* $\sqrt{s_{\rm NN}} = 2.76$ *TeV*, *Phys. Rev. Lett.* **107** (2011) 032301 [arXiv:1105.3865] [INSPIRE].

[21] ALICE collaboration, *Elliptic flow of identified hadrons in Pb-Pb collisions at* $\sqrt{s_{\rm NN}} = 2.76$ *TeV*, *JHEP* **06** (2015) 190 [arXiv:1405.4632] [INSPIRE].

[22] ALICE collaboration, *Anisotropic flow of charged particles in Pb-Pb collisions at* $\sqrt{s_{\rm NN}} = 5.02$ *TeV*, *Phys. Rev. Lett.* **116** (2016) 132302 [arXiv:1602.01119] [INSPIRE].

[23] ALICE collaboration, *Linear and non-linear flow modes in Pb-Pb collisions at* $\sqrt{s_{\rm NN}} = 2.76$ *TeV*, arXiv:1705.04377 [INSPIRE].

[24] ATLAS collaboration, *Measurement of the pseudorapidity and transverse momentum dependence of the elliptic flow of charged particles in lead-lead collisions at* $\sqrt{s_{\rm NN}} = 2.76$ *TeV with the ATLAS detector*, *Phys. Lett.* **B 707** (2012) 330 [arXiv:1108.6018] [INSPIRE].

[25] ATLAS collaboration, *Measurement of the azimuthal anisotropy for charged particle production in* $\sqrt{s_{\rm NN}} = 2.76$ *TeV lead-lead collisions with the ATLAS detector*, *Phys. Rev.* **C 86** (2012) 014907 [arXiv:1203.3087] [INSPIRE].

[26] ATLAS collaboration, *Measurement of the distributions of event-by-event flow harmonics in lead-lead collisions at* $= 2.76$ *TeV with the ATLAS detector at the LHC*, *JHEP* **11** (2013) 183 [arXiv:1305.2942] [INSPIRE].

[27] CMS collaboration, *Centrality dependence of dihadron correlations and azimuthal anisotropy harmonics in PbPb collisions at* $\sqrt{s_{\rm NN}} = 2.76$ *TeV*, *Eur. Phys. J.* **C 72** (2012) 2012 [arXiv:1201.3158] [INSPIRE].

[28] CMS collaboration, *Measurement of the elliptic anisotropy of charged particles produced in PbPb collisions at* $\sqrt{s_{\rm NN}} = 2.76$ *TeV*, *Phys. Rev.* **C 87** (2013) 014902 [arXiv:1204.1409] [INSPIRE].

[29] CMS collaboration, *Azimuthal anisotropy of charged particles at high transverse momenta in PbPb collisions at* $\sqrt{s_{\rm NN}} = 2.76$ *TeV*, *Phys. Rev. Lett.* **109** (2012) 022301 [arXiv:1204.1850] [INSPIRE].

JHEP09(2017)032

[30] ALICE collaboration, *Correlated event-by-event fluctuations of flow harmonics in Pb-Pb collisions at* $\sqrt{s_{\rm NN}} = 2.76$ *TeV*, *Phys. Rev. Lett.* **117** (2016) 182301 [arXiv:1604.07663] [INSPIRE].

[31] H. Song, Y. Zhou and K. Gajdosova, *Collective flow and hydrodynamics in large and small systems at the LHC*, *Nucl. Sci. Tech.* **28** (2017) 99 [arXiv:1703.00670] [INSPIRE].

[32] F.G. Gardim, F. Grassi, M. Luzum and J.-Y. Ollitrault, *Breaking of factorization of two-particle correlations in hydrodynamics*, *Phys. Rev.* **C 87** (2013) 031901 [arXiv:1211.0989] [INSPIRE].

[33] U. Heinz, Z. Qiu and C. Shen, *Fluctuating flow angles and anisotropic flow measurements*, *Phys. Rev.* **C 87** (2013) 034913 [arXiv:1302.3535] [INSPIRE].

[34] ALICE collaboration, *Harmonic decomposition of two-particle angular correlations in Pb-Pb collisions at* $\sqrt{s_{\rm NN}} = 2.76$ *TeV*, *Phys. Lett.* **B 708** (2012) 249 [arXiv:1109.2501] [INSPIRE].

[35] ALICE collaboration, *Long-range angular correlations on the near and away side in p-Pb collisions at* $\sqrt{s_{\rm NN}} = 5.02$ *TeV*, *Phys. Lett.* **B 719** (2013) 29 [arXiv:1212.2001] [INSPIRE].

[36] ALICE collaboration, *Long-range angular correlations of* π*,* K *and* p *in p-Pb collisions at* $\sqrt{s_{\rm NN}} = 5.02$ *TeV*, *Phys. Lett.* **B 726** (2013) 164 [arXiv:1307.3237] [INSPIRE].

[37] ALICE collaboration, *Multiplicity dependence of pion, kaon, proton and lambda production in p-Pb collisions at* $\sqrt{s_{\rm NN}} = 5.02$ *TeV*, *Phys. Lett.* **B 728** (2014) 25 [arXiv:1307.6796] [INSPIRE].

[38] ALICE collaboration, *Multiparticle azimuthal correlations in p-Pb and Pb-Pb collisions at the CERN Large Hadron Collider*, *Phys. Rev.* **C 90** (2014) 054901 [arXiv:1406.2474] [INSPIRE].

[39] ATLAS collaboration, *Observation of Associated Near-Side and Away-Side Long-Range Correlations in* $\sqrt{s_{\rm NN}} = 5.02$ *TeV Proton-Lead Collisions with the ATLAS Detector*, *Phys. Rev. Lett.* **110** (2013) 182302 [arXiv:1212.5198] [INSPIRE].

[40] ATLAS collaboration, *Measurement with the ATLAS detector of multi-particle azimuthal correlations in* $p + Pb$ *collisions at* $\sqrt{s_{\rm NN}} = 5.02$ *TeV*, *Phys. Lett.* **B 725** (2013) 60 [arXiv:1303.2084] [INSPIRE].

[41] CMS collaboration, *Studies of azimuthal dihadron correlations in ultra-central PbPb collisions at* $\sqrt{s_{\rm NN}} = 2.76$ *TeV*, *JHEP* **02** (2014) 088 [arXiv:1312.1845] [INSPIRE].

[42] CMS collaboration, *Multiplicity and transverse momentum dependence of two- and four-particle correlations in pPb and PbPb collisions*, *Phys. Lett.* **B 724** (2013) 213 [arXiv:1305.0609] [INSPIRE].

[43] CMS collaboration, *Study of the production of charged pions, kaons and protons in pPb collisions at* $\sqrt{s_{\rm NN}} = 5.02$ *TeV*, *Eur. Phys. J.* **C 74** (2014) 2847 [arXiv:1307.3442] [INSPIRE].

[44] CMS collaboration, *Long-range two-particle correlations of strange hadrons with charged particles in pPb and PbPb collisions at LHC energies*, *Phys. Lett.* **B 742** (2015) 200 [arXiv:1409.3392] [INSPIRE].

[45] CMS collaboration, *Evidence for Collective Multiparticle Correlations in p-Pb Collisions*, *Phys. Rev. Lett.* **115** (2015) 012301 [arXiv:1502.05382] [INSPIRE].

[46] LHCb collaboration, *Measurements of long-range near-side angular correlations in* $\sqrt{s_{\rm NN}} = 5$ *TeV proton-lead collisions in the forward region*, *Phys. Lett.* **B 762** (2016) 473 [arXiv:1512.00439] [INSPIRE].

JHEP09(2017)032

[47] CMS collaboration, *Evidence for transverse momentum and pseudorapidity dependent event plane fluctuations in PbPb and pPb collisions*, *Phys. Rev.* **C 92** (2015) 034911 [arXiv:1503.01692] [INSPIRE].

[48] L. Xu, L. Yi, D. Kikola, J. Konzer, F. Wang and W. Xie, *Model-independent decomposition of flow and nonflow in relativistic heavy-ion collisions*, *Phys. Rev.* **C 86** (2012) 024910 [arXiv:1204.2815] [INSPIRE].

[49] ALICE collaboration, *The ALICE experiment at the CERN LHC*, 2008 *JINST* **3** S08002 [INSPIRE].

[50] J. Alme et al., *The ALICE TPC, a large 3-dimensional tracking device with fast readout for ultra-high multiplicity events*, *Nucl. Instrum. Meth.* **A 622** (2010) 316 [arXiv:1001.1950] [INSPIRE].

[51] ALICE collaboration, *Alignment of the ALICE Inner Tracking System with cosmic-ray tracks*, 2010 *JINST* **5** P03003 [arXiv:1001.0502] [INSPIRE].

[52] ALICE collaboration, *Performance of the ALICE Experiment at the CERN LHC*, *Int. J. Mod. Phys.* **A 29** (2014) 1430044 [arXiv:1402.4476] [INSPIRE].

[53] ALICE collaboration, *Performance of the ALICE VZERO system*, 2013 *JINST* **8** P10016 [arXiv:1306.3130] [INSPIRE].

[54] ALICE collaboration, *Centrality determination of Pb-Pb collisions at* $\sqrt{s_{\rm NN}} = 2.76$ *TeV with ALICE*, *Phys. Rev.* **C 88** (2013) 044909 [arXiv:1301.4361] [INSPIRE].

[55] ALICE collaboration, *Pseudorapidity density of charged particles in* $p + Pb$ *collisions at* $\sqrt{s_{\rm NN}} = 5.02$ *TeV*, *Phys. Rev. Lett.* **110** (2013) 032301 [arXiv:1210.3615] [INSPIRE].

[56] M. Gyulassy and X.-N. Wang, *HIJING 1.0: A Monte Carlo program for parton and particle production in high-energy hadronic and nuclear collisions*, *Comput. Phys. Commun.* **83** (1994) 307 [nucl-th/9502021] [INSPIRE].

[57] Z.-W. Lin, C.M. Ko, B.-A. Li, B. Zhang and S. Pal, *A Multi-phase transport model for relativistic heavy ion collisions*, *Phys. Rev.* **C 72** (2005) 064901 [nucl-th/0411110] [INSPIRE].

[58] R. Brun et al., *GEANT Detector Description and Simulation Tool*, CERN-W-5013 (1994) [INSPIRE].

[59] S. Roesler, R. Engel and J. Ranft, *The Monte Carlo event generator DPMJET-III*, in proceedings of the *International Conference on Advanced Monte Carlo for Radiation Physics, Particle Transport Simulation and Applications (MC 2000)*, Lisbon, Portugal, 23–26 October 2000, Springer (2000), pp. 1033–1038 http://www-public.slac.stanford.edu/sciDoc/docMeta.aspx?slacPubNumber=SLAC-PUB-8740 [hep-ph/0012252] [INSPIRE].

[60] W. Zhao, H.-j. Xu and H. Song, *Collective flow in* 2.76 *A TeV and* 5.02 *A TeV* $Pb + Pb$ *collisions*, arXiv:1703.10792 [INSPIRE].

[61] Z. Qiu, C. Shen and U. Heinz, *Hydrodynamic elliptic and triangular flow in Pb-Pb collisions at* $\sqrt{s} = 2.76$ *A TeV*, *Phys. Lett.* **B 707** (2012) 151 [arXiv:1110.3033] [INSPIRE].

[62] I. Kozlov, M. Luzum, G. Denicol, S. Jeon and C. Gale, *Transverse momentum structure of pair correlations as a signature of collective behavior in small collision systems*, arXiv:1405.3976 [INSPIRE].

[63] ALICE collaboration, *Multiplicity dependence of the average transverse momentum in pp, p-Pb and Pb-Pb collisions at the LHC*, *Phys. Lett.* **B 727** (2013) 371 [arXiv:1307.1094] [INSPIRE].

JHEP09(2017)032

The ALICE collaboration

S. Acharya[139], D. Adamová[96], J. Adolfsson[34], M.M. Aggarwal[101], G. Aglieri Rinella[35], M. Agnello[31], N. Agrawal[48], Z. Ahammed[139], N. Ahmad[17], S.U. Ahn[80], S. Aiola[143], A. Akindinov[65], S.N. Alam[139], J.L.B. Alba[114], D.S.D. Albuquerque[125], D. Aleksandrov[92], B. Alessandro[59], R. Alfaro Molina[75], A. Alici[54,27,12], A. Alkin[3], J. Alme[22], T. Alt[71], L. Altenkamper[22], I. Altsybeev[138], C. Alves Garcia Prado[124], C. Andrei[89], D. Andreou[35], H.A. Andrews[113], A. Andronic[109], V. Anguelov[106], C. Anson[99], T. Antičić[110], F. Antinori[57], P. Antonioli[54], R. Anwar[127], L. Aphecetche[117], H. Appelshäuser[71], S. Arcelli[27], R. Arnaldi[59], O.W. Arnold[107,36], I.C. Arsene[21], M. Arslandok[106], B. Audurier[117], A. Augustinus[35], R. Averbeck[109], M.D. Azmi[17], A. Badalà[56], Y.W. Baek[61,79], S. Bagnasco[59], R. Bailhache[71], R. Bala[103], A. Baldisseri[76], M. Ball[45], R.C. Baral[68], A.M. Barbano[26], R. Barbera[28], F. Barile[33,53], L. Barioglio[26], G.G. Barnaföldi[142], L.S. Barnby[95], V. Barret[82], P. Bartalini[7], K. Barth[35], E. Bartsch[71], M. Basile[27], N. Bastid[82], S. Basu[141], B. Bathen[72], G. Batigne[117], B. Batyunya[78], P.C. Batzing[21], I.G. Bearden[93], H. Beck[106], C. Bedda[64], N.K. Behera[61], I. Belikov[135], F. Bellini[27], H. Bello Martinez[2], R. Bellwied[127], L.G.E. Beltran[123], V. Belyaev[85], G. Bencedi[142], S. Beole[26], A. Bercuci[89], Y. Berdnikov[98], D. Berenyi[142], R.A. Bertens[130], D. Berzano[35], L. Betev[35], A. Bhasin[103], I.R. Bhat[103], A.K. Bhati[101], B. Bhattacharjee[44], J. Bhom[121], L. Bianchi[127], N. Bianchi[51], C. Bianchin[141], J. Bielčík[39], J. Bielčíková[96], A. Bilandzic[36,107], G. Biro[142], R. Biswas[4], S. Biswas[4], J.T. Blair[122], D. Blau[92], C. Blume[71], G. Boca[136], F. Bock[106,84,35], A. Bogdanov[85], L. Boldizsár[142], M. Bombara[40], G. Bonomi[137], M. Bonora[35], J. Book[71], H. Borel[76], A. Borissov[19], M. Borri[129], E. Botta[26], C. Bourjau[93], L. Bratrud[71], P. Braun-Munzinger[109], M. Bregant[124], T.A. Broker[71], M. Broz[39], E.J. Brucken[46], E. Bruna[59], G.E. Bruno[33], D. Budnikov[111], H. Buesching[71], S. Bufalino[31], P. Buhler[116], P. Buncic[35], O. Busch[133], Z. Buthelezi[77], J.B. Butt[15], J.T. Buxton[18], J. Cabala[119], D. Caffarri[35,94], H. Caines[143], A. Caliva[64], E. Calvo Villar[114], P. Camerini[25], A.A. Capon[116], F. Carena[35], W. Carena[35], F. Carnesecchi[27,12], J. Castillo Castellanos[76], A.J. Castro[130], E.A.R. Casula[24,55], C. Ceballos Sanchez[9], P. Cerello[59], S. Chandra[139], B. Chang[128], S. Chapeland[35], M. Chartier[129], J.L. Charvet[76], S. Chattopadhyay[139], S. Chattopadhyay[112], A. Chauvin[36,107], M. Cherney[99], C. Cheshkov[134], B. Cheynis[134], V. Chibante Barroso[35], D.D. Chinellato[125], S. Cho[61], P. Chochula[35], K. Choi[19], M. Chojnacki[93], S. Choudhury[139], T. Chowdhury[82], P. Christakoglou[94], C.H. Christensen[93], P. Christiansen[34], T. Chujo[133], S.U. Chung[19], C. Cicalo[55], L. Cifarelli[12,27], F. Cindolo[54], J. Cleymans[102], F. Colamaria[33], D. Colella[35,66], A. Collu[84], M. Colocci[27], M. Concas[59, ii], G. Conesa Balbastre[83], Z. Conesa del Valle[62], M.E. Connors[143, iii], J.G. Contreras[39], T.M. Cormier[97], Y. Corrales Morales[59], I. Cortés Maldonado[2], P. Cortese[32], M.R. Cosentino[126], F. Costa[35], S. Costanza[136], J. Crkovská[62], P. Crochet[82], E. Cuautle[73], L. Cunqueiro[72], T. Dahms[36,107], A. Dainese[57], M.C. Danisch[106], A. Danu[69], D. Das[112], I. Das[112], S. Das[4], A. Dash[90], S. Dash[48], S. De[124,49], A. De Caro[30], G. de Cataldo[53], C. de Conti[124], J. de Cuveland[42], A. De Falco[24], D. De Gruttola[30,12], N. De Marco[59], S. De Pasquale[30], R.D. De Souza[125], H.F. Degenhardt[124], A. Deisting[109,106], A. Deloff[88], C. Deplano[94], P. Dhankher[48], D. Di Bari[33], A. Di Mauro[35], P. Di Nezza[51], B. Di Ruzza[57], M.A. Diaz Corchero[10], T. Dietel[102], P. Dillenseger[71], R. Divià[35], Ø. Djuvsland[22], A. Dobrin[35], D. Domenicis Gimenez[124], B. Dönigus[71], O. Dordic[21], L.V.V. Doremalen[64], T. Drozhzhova[71], A.K. Dubey[139], A. Dubla[109], L. Ducroux[134], A.K. Duggal[101], P. Dupieux[82], R.J. Ehlers[143], D. Elia[53], E. Endress[114], H. Engel[70], E. Epple[143], B. Erazmus[117], F. Erhardt[100], B. Espagnon[62], S. Esumi[133], G. Eulisse[35], J. Eum[19], D. Evans[113], S. Evdokimov[115], L. Fabbietti[107,36], J. Faivre[83], A. Fantoni[51], M. Fasel[97,84], L. Feldkamp[72], A. Feliciello[59], G. Feofilov[138], J. Ferencei[96], A. Fernández Téllez[2], E.G. Ferreiro[16], A. Ferretti[26], A. Festanti[29,35], V.J.G. Feuillard[76,82], J. Figiel[121], M.A.S. Figueredo[124], S. Filchagin[111], D. Finogeev[63],

JHEP09(2017)032

F.M. Fionda[22,24], E.M. Fiore[33], M. Floris[35], S. Foertsch[77], P. Foka[109], S. Fokin[92], E. Fragiacomo[60], A. Francescon[35], A. Francisco[117], U. Frankenfeld[109], G.G. Fronze[26], U. Fuchs[35], C. Furget[83], A. Furs[63], M. Fusco Girard[30], J.J. Gaardhøje[93], M. Gagliardi[26], A.M. Gago[114], K. Gajdosova[93], M. Gallio[26], C.D. Galvan[123], P. Ganoti[87], C. Gao[7], C. Garabatos[109], E. Garcia-Solis[13], K. Garg[28], P. Garg[49], C. Gargiulo[35], P. Gasik[107,36], E.F. Gauger[122], M.B. Gay Ducati[74], M. Germain[117], J. Ghosh[112], P. Ghosh[139], S.K. Ghosh[4], P. Gianotti[51], P. Giubellino[109,59,35], P. Giubilato[29], E. Gladysz-Dziadus[121], P. Glässel[106], D.M. Goméz Coral[75], A. Gomez Ramirez[70], A.S. Gonzalez[35], V. Gonzalez[10], P. González-Zamora[10], S. Gorbunov[42], L. Görlich[121], S. Gotovac[120], V. Grabski[75], L.K. Graczykowski[140], K.L. Graham[113], L. Greiner[84], A. Grelli[64], C. Grigoras[35], V. Grigoriev[85], A. Grigoryan[1], S. Grigoryan[78], N. Grion[60], J.M. Gronefeld[109], F. Grosa[31], J.F. Grosse-Oetringhaus[35], R. Grosso[109], L. Gruber[116], F. Guber[63], R. Guernane[83], B. Guerzoni[27], K. Gulbrandsen[93], T. Gunji[132], A. Gupta[103], R. Gupta[103], I.B. Guzman[2], R. Haake[35], C. Hadjidakis[62], H. Hamagaki[86,132], G. Hamar[142], J.C. Hamon[135], M.R. Haque[64], J.W. Harris[143], A. Harton[13], H. Hassan[83], D. Hatzifotiadou[12,54], S. Hayashi[132], S.T. Heckel[71], E. Hellbär[71], H. Helstrup[37], A. Herghelegiu[89], G. Herrera Corral[11], F. Herrmann[72], B.A. Hess[105], K.F. Hetland[37], H. Hillemanns[35], C. Hills[129], B. Hippolyte[135], J. Hladky[67], B. Hohlweger[107], D. Horak[39], S. Hornung[109], R. Hosokawa[133,83], P. Hristov[35], C. Hughes[130], T.J. Humanic[18], N. Hussain[44], T. Hussain[17], D. Hutter[42], D.S. Hwang[20], S.A. Iga Buitron[73], R. Ilkaev[111], M. Inaba[133], M. Ippolitov[85,92], M. Irfan[17], V. Isakov[63], M. Ivanov[109], V. Ivanov[98], V. Izucheev[115], B. Jacak[84], N. Jacazio[27], P.M. Jacobs[84], M.B. Jadhav[48], S. Jadlovska[119], J. Jadlovsky[119], S. Jaelani[64], C. Jahnke[36], M.J. Jakubowska[140], M.A. Janik[140], P.H.S.Y. Jayarathna[127], C. Jena[90], S. Jena[127], M. Jercic[100], R.T. Jimenez Bustamante[109], P.G. Jones[113], A. Jusko[113], P. Kalinak[66], A. Kalweit[35], J.H. Kang[144], V. Kaplin[85], S. Kar[139], A. Karasu Uysal[81], O. Karavichev[63], T. Karavicheva[63], L. Karayan[106,109], P. Karczmarczyk[35], E. Karpechev[63], U. Kebschull[70], R. Keidel[145], D.L.D. Keijdener[64], M. Keil[35], B. Ketzer[45], Z. Khabanova[94], P. Khan[112], S.A. Khan[139], A. Khanzadeev[98], Y. Kharlov[115], A. Khatun[17], A. Khuntia[49], M.M. Kielbowicz[121], B. Kileng[37], B. Kim[133], D. Kim[144], D.W. Kim[43], D.J. Kim[128], H. Kim[144], J.S. Kim[43], J. Kim[106], M. Kim[61], M. Kim[144], S. Kim[20], T. Kim[144], S. Kirsch[42], I. Kisel[42], S. Kiselev[65], A. Kisiel[140], G. Kiss[142], J.L. Klay[6], C. Klein[71], J. Klein[35], C. Klein-Bösing[72], S. Klewin[106], A. Kluge[35], M.L. Knichel[106], A.G. Knospe[127], C. Kobdaj[118], M. Kofarago[142], T. Kollegger[109], A. Kolojvari[138], V. Kondratiev[138], N. Kondratyeva[85], E. Kondratyuk[115], A. Konevskikh[63], M. Konyushikhin[141], M. Kopcik[119], M. Kour[103], C. Kouzinopoulos[35], O. Kovalenko[88], V. Kovalenko[138], M. Kowalski[121], G. Koyithatta Meethaleveedu[48], I. Králik[66], A. Kravčáková[40], M. Krivda[66,113], F. Krizek[96], E. Kryshen[98], M. Krzewicki[42], A.M. Kubera[18], V. Kučera[96], C. Kuhn[135], P.G. Kuijer[94], A. Kumar[103], J. Kumar[48], L. Kumar[101], S. Kumar[48], S. Kundu[90], P. Kurashvili[88], A. Kurepin[63], A.B. Kurepin[63], A. Kuryakin[111], S. Kushpil[96], M.J. Kweon[61], Y. Kwon[144], S.L. La Pointe[42], P. La Rocca[28], C. Lagana Fernandes[124], Y.S. Lai[84], I. Lakomov[35], R. Langoy[41], K. Lapidus[143], C. Lara[70], A. Lardeux[21,76], A. Lattuca[26], E. Laudi[35], R. Lavicka[39], L. Lazaridis[35], R. Lea[25], L. Leardini[106], S. Lee[144], F. Lehas[94], S. Lehner[116], J. Lehrbach[42], R.C. Lemmon[95], V. Lenti[53], E. Leogrande[64], I. León Monzón[123], P. Lévai[142], S. Li[7], X. Li[14], J. Lien[41], R. Lietava[113], B. Lim[19], S. Lindal[21], V. Lindenstruth[42], S.W. Lindsay[129], C. Lippmann[109], M.A. Lisa[18], V. Litichevskyi[46], H.M. Ljunggren[34], W.J. Llope[141], D.F. Lodato[64], P.I. Loenne[22], V. Loginov[85], C. Loizides[84], P. Loncar[120], X. Lopez[82], E. López Torres[9], A. Lowe[142], P. Luettig[71], M. Lunardon[29], G. Luparello[25], M. Lupi[35], T.H. Lutz[143], A. Maevskaya[63], M. Mager[35], S. Mahajan[103], S.M. Mahmood[21], A. Maire[135], R.D. Majka[143], M. Malaev[98], L. Malinina[78, iv], D. Mal'Kevich[65], P. Malzacher[109], A. Mamonov[111], V. Manko[92], F. Manso[82], V. Manzari[53], Y. Mao[7], M. Marchisone[77,131], J. Mareš[67], G.V. Margagliotti[25], A. Margotti[54], J. Margutti[64], A. Marín[109], C. Markert[122], M. Marquard[71], N.A. Martin[109], P. Martinengo[35],

JHEP09(2017)032

J.A.L. Martinez[70], M.I. Martínez[2], G. Martínez García[117], M. Martinez Pedreira[35], A. Mas[124], S. Masciocchi[109], M. Masera[26], A. Masoni[55], E. Masson[117], A. Mastroserio[33], A.M. Mathis[107,36], A. Matyja[121,130], C. Mayer[121], J. Mazer[130], M. Mazzilli[33], M.A. Mazzoni[58], F. Meddi[23], Y. Melikyan[85], A. Menchaca-Rocha[75], E. Meninno[30], J. Mercado Pérez[106], M. Meres[38], S. Mhlanga[102], Y. Miake[133], M.M. Mieskolainen[46], D. Mihaylov[107], D.L. Mihaylov[107], K. Mikhaylov[65,78], L. Milano[84], J. Milosevic[21], A. Mischke[64], A.N. Mishra[49], D. Miśkowiec[109], J. Mitra[139], C.M. Mitu[69], N. Mohammadi[64], B. Mohanty[90], M. Mohisin Khan[17, v], E. Montes[10], D.A. Moreira De Godoy[72], L.A.P. Moreno[2], S. Moretto[29], A. Morreale[117], A. Morsch[35], V. Muccifora[51], E. Mudnic[120], D. Mühlheim[72], S. Muhuri[139], M. Mukherjee[4], J.D. Mulligan[143], M.G. Munhoz[124], K. Münning[45], R.H. Munzer[71], H. Murakami[132], S. Murray[77], L. Musa[35], J. Musinsky[66], C.J. Myers[127], J.W. Myrcha[140], B. Naik[48], R. Nair[88], B.K. Nandi[48], R. Nania[54,12], E. Nappi[53], A. Narayan[48], M.U. Naru[15], H. Natal da Luz[124], C. Nattrass[130], S.R. Navarro[2], K. Nayak[90], R. Nayak[48], T.K. Nayak[139], S. Nazarenko[111], A. Nedosekin[65], R.A. Negrao De Oliveira[35], L. Nellen[73], S.V. Nesbo[37], F. Ng[127], M. Nicassio[109], M. Niculescu[69], J. Niedziela[140,35], B.S. Nielsen[93], S. Nikolaev[92], S. Nikulin[92], V. Nikulin[98], A. Nobuhiro[47], F. Noferini[12,54], P. Nomokonov[78], G. Nooren[64], J.C.C. Noris[2], J. Norman[129], A. Nyanin[92], J. Nystrand[22], H. Oeschler[106, i], S. Oh[143], A. Ohlson[106,35], T. Okubo[47], L. Olah[142], J. Oleniacz[140], A.C. Oliveira Da Silva[124], M.H. Oliver[143], J. Onderwaater[109], C. Oppedisano[59], R. Orava[46], M. Oravec[119], A. Ortiz Velasquez[73], A. Oskarsson[34], J. Otwinowski[121], K. Oyama[86], Y. Pachmayer[106], V. Pacik[93], D. Pagano[137], P. Pagano[30], G. Paić[73], P. Palni[7], J. Pan[141], A.K. Pandey[48], S. Panebianco[76], V. Papikyan[1], G.S. Pappalardo[56], P. Pareek[49], J. Park[61], S. Parmar[101], A. Passfeld[72], S.P. Pathak[127], V. Paticchio[53], R.N. Patra[139], B. Paul[59], H. Pei[7], T. Peitzmann[64], X. Peng[7], L.G. Pereira[74], H. Pereira Da Costa[76], D. Peresunko[92,85], E. Perez Lezama[71], V. Peskov[71], Y. Pestov[5], V. Petráček[39], V. Petrov[115], M. Petrovici[89], C. Petta[28], R.P. Pezzi[74], S. Piano[60], M. Pikna[38], P. Pillot[117], L.O.D.L. Pimentel[93], O. Pinazza[35,54], L. Pinsky[127], D.B. Piyarathna[127], M. Płoskoń[84], M. Planinic[100], F. Pliquett[71], J. Pluta[140], S. Pochybova[142], P.L.M. Podesta-Lerma[123], M.G. Poghosyan[97], B. Polichtchouk[115], N. Poljak[100], W. Poonsawat[118], A. Pop[89], H. Poppenborg[72], S. Porteboeuf-Houssais[82], J. Porter[84], V. Pozdniakov[78], S.K. Prasad[4], R. Preghenella[54,35], F. Prino[59], C.A. Pruneau[141], I. Pshenichnov[63], M. Puccio[26], G. Puddu[24], P. Pujahari[141], V. Punin[111], J. Putschke[141], A. Rachevski[60], S. Raha[4], S. Rajput[103], J. Rak[128], A. Rakotozafindrabe[76], L. Ramello[32], F. Rami[135], D.B. Rana[127], R. Raniwala[104], S. Raniwala[104], S.S. Räsänen[46], B.T. Rascanu[71], D. Rathee[101], V. Ratza[45], I. Ravasenga[31], K.F. Read[97,130], K. Redlich[88, vi], A. Rehman[22], P. Reichelt[71], F. Reidt[35], X. Ren[7], R. Renfordt[71], A.R. Reolon[51], A. Reshetin[63], K. Reygers[106], V. Riabov[98], R.A. Ricci[52], T. Richert[64], M. Richter[21], P. Riedler[35], W. Riegler[35], F. Riggi[28], C. Ristea[69], M. Rodríguez Cahuantzi[2], K. Røed[21], E. Rogochaya[78], D. Rohr[35,42], D. Röhrich[22], P.S. Rokita[140], F. Ronchetti[51], E.D. Rosas[73], P. Rosnet[82], A. Rossi[29], A. Rotondi[136], F. Roukoutakis[87], A. Roy[49], C. Roy[135], P. Roy[112], A.J. Rubio Montero[10], O.V. Rueda[73], R. Rui[25], B. Rumyantsev[78], A. Rustamov[91], E. Ryabinkin[92], Y. Ryabov[98], A. Rybicki[121], S. Saarinen[46], S. Sadhu[139], S. Sadovsky[115], K. Šafařík[35], S.K. Saha[139], B. Sahlmuller[71], B. Sahoo[48], P. Sahoo[49], R. Sahoo[49], S. Sahoo[68], P.K. Sahu[68], J. Saini[139], S. Sakai[51,133], M.A. Saleh[141], J. Salzwedel[18], S. Sambyal[103], V. Samsonov[85,98], A. Sandoval[75], D. Sarkar[139], N. Sarkar[139], P. Sarma[44], M.H.P. Sas[64], E. Scapparone[54], F. Scarlassara[29], R.P. Scharenberg[108], H.S. Scheid[71], C. Schiaua[89], R. Schicker[106], C. Schmidt[109], H.R. Schmidt[105], M.O. Schmidt[106], M. Schmidt[105], S. Schuchmann[106], J. Schukraft[35], Y. Schutz[35,135,117], K. Schwarz[109], K. Schweda[109], G. Scioli[27], E. Scomparin[59], R. Scott[130], M. Šefčík[40], J.E. Seger[99], Y. Sekiguchi[132], D. Sekihata[47], I. Selyuzhenkov[85,109], K. Senosi[77], S. Senyukov[35,135,3], E. Serradilla[75,10], P. Sett[48], A. Sevcenco[69], A. Shabanov[63], A. Shabetai[117], R. Shahoyan[35], W. Shaikh[112], A. Shangaraev[115], A. Sharma[101], A. Sharma[103], M. Sharma[103], M. Sharma[103],

JHEP09(2017)032

N. Sharma[101,130], A.I. Sheikh[139], K. Shigaki[47], Q. Shou[7], K. Shtejer[9,26], Y. Sibiriak[92], S. Siddhanta[55], K.M. Sielewicz[35], T. Siemiarczuk[88], D. Silvermyr[34], C. Silvestre[83], G. Simatovic[100], G. Simonetti[35], R. Singaraju[139], R. Singh[90], V. Singhal[139], T. Sinha[112], B. Sitar[38], M. Sitta[32], T.B. Skaali[21], M. Slupecki[128], N. Smirnov[143], R.J.M. Snellings[64], T.W. Snellman[128], J. Song[19], M. Song[144], F. Soramel[29], S. Sorensen[130], F. Sozzi[109], E. Spiriti[51], I. Sputowska[121], B.K. Srivastava[108], J. Stachel[106], I. Stan[69], P. Stankus[97], E. Stenlund[34], D. Stocco[117], P. Strmen[38], A.A.P. Suaide[124], T. Sugitate[47], C. Suire[62], M. Suleymanov[15], M. Suljic[25], R. Sultanov[65], M. Šumbera[96], S. Sumowidagdo[50], K. Suzuki[116], S. Swain[68], A. Szabo[38], I. Szarka[38], U. Tabassam[15], J. Takahashi[125], G.J. Tambave[22], N. Tanaka[133], M. Tarhini[62], M. Tariq[17], M.G. Tarzila[89], A. Tauro[35], G. Tejeda Muñoz[2], A. Telesca[35], K. Terasaki[132], C. Terrevoli[29], B. Teyssier[134], D. Thakur[49], S. Thakur[139], D. Thomas[122], F. Thoresen[93], R. Tieulent[134], A. Tikhonov[63], A.R. Timmins[127], A. Toia[71], S. Tripathy[49], S. Trogolo[26], G. Trombetta[33], L. Tropp[40], V. Trubnikov[3], W.H. Trzaska[128], B.A. Trzeciak[64], T. Tsuji[132], A. Tumkin[111], R. Turrisi[57], T.S. Tveter[21], K. Ullaland[22], E.N. Umaka[127], A. Uras[134], G.L. Usai[24], A. Utrobicic[100], M. Vala[66,119], J. Van Der Maarel[64], J.W. Van Hoorne[35], M. van Leeuwen[64], T. Vanat[96], P. Vande Vyvre[35], D. Varga[142], A. Vargas[2], M. Vargyas[128], R. Varma[48], M. Vasileiou[87], A. Vasiliev[92], A. Vauthier[83], O. Vázquez Doce[107,36], V. Vechernin[138], A.M. Veen[64], A. Velure[22], E. Vercellin[26], S. Vergara Limón[2], R. Vernet[8], R. Vértesi[142], L. Vickovic[120], S. Vigolo[64], J. Viinikainen[128], Z. Vilakazi[131], O. Villalobos Baillie[113], A. Villatoro Tello[2], A. Vinogradov[92], L. Vinogradov[138], T. Virgili[30], V. Vislavicius[34], A. Vodopyanov[78], M.A. Völkl[106,105], K. Voloshin[65], S.A. Voloshin[141], G. Volpe[33], B. von Haller[35], I. Vorobyev[36,107], D. Voscek[119], D. Vranic[35,109], J. Vrláková[40], B. Wagner[22], H. Wang[64], M. Wang[7], D. Watanabe[133], Y. Watanabe[132], M. Weber[116], S.G. Weber[109], D.F. Weiser[106], S.C. Wenzel[35], J.P. Wessels[72], U. Westerhoff[72], A.M. Whitehead[102], J. Wiechula[71], J. Wikne[21], G. Wilk[88], J. Wilkinson[106,54], G.A. Willems[72], M.C.S. Williams[54], E. Willsher[113], B. Windelband[106], W.E. Witt[130], S. Yalcin[81], K. Yamakawa[47], P. Yang[7], S. Yano[47], Z. Yin[7], H. Yokoyama[133,83], I.-K. Yoo[35,19], J.H. Yoon[61], V. Yurchenko[3], V. Zaccolo[59,93], A. Zaman[15], C. Zampolli[35], H.J.C. Zanoli[124], N. Zardoshti[113], A. Zarochentsev[138], P. Závada[67], N. Zaviyalov[111], H. Zbroszczyk[140], M. Zhalov[98], H. Zhang[22,7], X. Zhang[7], Y. Zhang[7], C. Zhang[64], Z. Zhang[7,82], C. Zhao[21], N. Zhigareva[65], D. Zhou[7], Y. Zhou[93], Z. Zhou[22], H. Zhu[22], J. Zhu[7], X. Zhu[7], A. Zichichi[12,27], A. Zimmermann[106], M.B. Zimmermann[35,72], G. Zinovjev[3], J. Zmeskal[116], S. Zou[7]

[i] *Deceased*
[ii] *Also at: Dipartimento DET del Politecnico di Torino, Turin, Italy*
[iii] *Also at: Georgia State University, Atlanta, Georgia, United States*
[iv] *Also at: M.V. Lomonosov Moscow State University, D.V. Skobeltsyn Institute of Nuclear, Physics, Moscow, Russia*
[v] *Also at: Department of Applied Physics, Aligarh Muslim University, Aligarh, India*
[vi] *Also at: Institute of Theoretical Physics, University of Wroclaw, Poland*

[1] *A.I. Alikhanyan National Science Laboratory (Yerevan Physics Institute) Foundation, Yerevan, Armenia*
[2] *Benemérita Universidad Autónoma de Puebla, Puebla, Mexico*
[3] *Bogolyubov Institute for Theoretical Physics, Kiev, Ukraine*
[4] *Bose Institute, Department of Physics and Centre for Astroparticle Physics and Space Science (CAPSS), Kolkata, India*
[5] *Budker Institute for Nuclear Physics, Novosibirsk, Russia*

JHEP09(2017)032

[6] California Polytechnic State University, San Luis Obispo, California, United States
[7] Central China Normal University, Wuhan, China
[8] Centre de Calcul de l'IN2P3, Villeurbanne, Lyon, France
[9] Centro de Aplicaciones Tecnológicas y Desarrollo Nuclear (CEADEN), Havana, Cuba
[10] Centro de Investigaciones Energéticas Medioambientales y Tecnológicas (CIEMAT), Madrid, Spain
[11] Centro de Investigación y de Estudios Avanzados (CINVESTAV), Mexico City and Mérida, Mexico
[12] Centro Fermi - Museo Storico della Fisica e Centro Studi e Ricerche "Enrico Fermi', Rome, Italy
[13] Chicago State University, Chicago, Illinois, United States
[14] China Institute of Atomic Energy, Beijing, China
[15] COMSATS Institute of Information Technology (CIIT), Islamabad, Pakistan
[16] Departamento de Física de Partículas and IGFAE, Universidad de Santiago de Compostela, Santiago de Compostela, Spain
[17] Department of Physics, Aligarh Muslim University, Aligarh, India
[18] Department of Physics, Ohio State University, Columbus, Ohio, United States
[19] Department of Physics, Pusan National University, Pusan, South Korea
[20] Department of Physics, Sejong University, Seoul, South Korea
[21] Department of Physics, University of Oslo, Oslo, Norway
[22] Department of Physics and Technology, University of Bergen, Bergen, Norway
[23] Dipartimento di Fisica dell'Università 'La Sapienza' and Sezione INFN, Rome, Italy
[24] Dipartimento di Fisica dell'Università and Sezione INFN, Cagliari, Italy
[25] Dipartimento di Fisica dell'Università and Sezione INFN, Trieste, Italy
[26] Dipartimento di Fisica dell'Università and Sezione INFN, Turin, Italy
[27] Dipartimento di Fisica e Astronomia dell'Università and Sezione INFN, Bologna, Italy
[28] Dipartimento di Fisica e Astronomia dell'Università and Sezione INFN, Catania, Italy
[29] Dipartimento di Fisica e Astronomia dell'Università and Sezione INFN, Padova, Italy
[30] Dipartimento di Fisica 'E.R. Caianiello' dell'Università and Gruppo Collegato INFN, Salerno, Italy
[31] Dipartimento DISAT del Politecnico and Sezione INFN, Turin, Italy
[32] Dipartimento di Scienze e Innovazione Tecnologica dell'Università del Piemonte Orientale and INFN Sezione di Torino, Alessandria, Italy
[33] Dipartimento Interateneo di Fisica 'M. Merlin' and Sezione INFN, Bari, Italy
[34] Division of Experimental High Energy Physics, University of Lund, Lund, Sweden
[35] European Organization for Nuclear Research (CERN), Geneva, Switzerland
[36] Excellence Cluster Universe, Technische Universität München, Munich, Germany
[37] Faculty of Engineering, Bergen University College, Bergen, Norway
[38] Faculty of Mathematics, Physics and Informatics, Comenius University, Bratislava, Slovakia
[39] Faculty of Nuclear Sciences and Physical Engineering, Czech Technical University in Prague, Prague, Czech Republic
[40] Faculty of Science, P.J. Šafárik University, Košice, Slovakia
[41] Faculty of Technology, Buskerud and Vestfold University College, Tonsberg, Norway
[42] Frankfurt Institute for Advanced Studies, Johann Wolfgang Goethe-Universität Frankfurt, Frankfurt, Germany
[43] Gangneung-Wonju National University, Gangneung, South Korea
[44] Gauhati University, Department of Physics, Guwahati, India
[45] Helmholtz-Institut für Strahlen- und Kernphysik, Rheinische Friedrich-Wilhelms-Universität Bonn, Bonn, Germany
[46] Helsinki Institute of Physics (HIP), Helsinki, Finland
[47] Hiroshima University, Hiroshima, Japan
[48] Indian Institute of Technology Bombay (IIT), Mumbai, India
[49] Indian Institute of Technology Indore, Indore, India
[50] Indonesian Institute of Sciences, Jakarta, Indonesia
[51] INFN, Laboratori Nazionali di Frascati, Frascati, Italy
[52] INFN, Laboratori Nazionali di Legnaro, Legnaro, Italy
[53] INFN, Sezione di Bari, Bari, Italy

JHEP09(2017)032

[54] INFN, Sezione di Bologna, Bologna, Italy
[55] INFN, Sezione di Cagliari, Cagliari, Italy
[56] INFN, Sezione di Catania, Catania, Italy
[57] INFN, Sezione di Padova, Padova, Italy
[58] INFN, Sezione di Roma, Rome, Italy
[59] INFN, Sezione di Torino, Turin, Italy
[60] INFN, Sezione di Trieste, Trieste, Italy
[61] Inha University, Incheon, South Korea
[62] Institut de Physique Nucléaire d'Orsay (IPNO), Université Paris-Sud, CNRS-IN2P3, Orsay, France
[63] Institute for Nuclear Research, Academy of Sciences, Moscow, Russia
[64] Institute for Subatomic Physics of Utrecht University, Utrecht, Netherlands
[65] Institute for Theoretical and Experimental Physics, Moscow, Russia
[66] Institute of Experimental Physics, Slovak Academy of Sciences, Košice, Slovakia
[67] Institute of Physics, Academy of Sciences of the Czech Republic, Prague, Czech Republic
[68] Institute of Physics, Bhubaneswar, India
[69] Institute of Space Science (ISS), Bucharest, Romania
[70] Institut für Informatik, Johann Wolfgang Goethe-Universität Frankfurt, Frankfurt, Germany
[71] Institut für Kernphysik, Johann Wolfgang Goethe-Universität Frankfurt, Frankfurt, Germany
[72] Institut für Kernphysik, Westfälische Wilhelms-Universität Münster, Münster, Germany
[73] Instituto de Ciencias Nucleares, Universidad Nacional Autónoma de México, Mexico City, Mexico
[74] Instituto de Física, Universidade Federal do Rio Grande do Sul (UFRGS), Porto Alegre, Brazil
[75] Instituto de Física, Universidad Nacional Autónoma de México, Mexico City, Mexico
[76] IRFU, CEA, Université Paris-Saclay, Saclay, France
[77] iThemba LABS, National Research Foundation, Somerset West, South Africa
[78] Joint Institute for Nuclear Research (JINR), Dubna, Russia
[79] Konkuk University, Seoul, South Korea
[80] Korea Institute of Science and Technology Information, Daejeon, South Korea
[81] KTO Karatay University, Konya, Turkey
[82] Laboratoire de Physique Corpusculaire (LPC), Clermont Université, Université Blaise Pascal, CNRS–IN2P3, Clermont-Ferrand, France
[83] Laboratoire de Physique Subatomique et de Cosmologie, Université Grenoble-Alpes, CNRS-IN2P3, Grenoble, France
[84] Lawrence Berkeley National Laboratory, Berkeley, California, United States
[85] Moscow Engineering Physics Institute, Moscow, Russia
[86] Nagasaki Institute of Applied Science, Nagasaki, Japan
[87] National and Kapodistrian University of Athens, Physics Department, Athens, Greece
[88] National Centre for Nuclear Studies, Warsaw, Poland
[89] National Institute for Physics and Nuclear Engineering, Bucharest, Romania
[90] National Institute of Science Education and Research, Bhubaneswar, India
[91] National Nuclear Research Center, Baku, Azerbaijan
[92] National Research Centre Kurchatov Institute, Moscow, Russia
[93] Niels Bohr Institute, University of Copenhagen, Copenhagen, Denmark
[94] Nikhef, Nationaal instituut voor subatomaire fysica, Amsterdam, Netherlands
[95] Nuclear Physics Group, STFC Daresbury Laboratory, Daresbury, United Kingdom
[96] Nuclear Physics Institute, Academy of Sciences of the Czech Republic, Řež u Prahy, Czech Republic
[97] Oak Ridge National Laboratory, Oak Ridge, Tennessee, United States
[98] Petersburg Nuclear Physics Institute, Gatchina, Russia
[99] Physics Department, Creighton University, Omaha, Nebraska, United States
[100] Physics department, Faculty of science, University of Zagreb, Zagreb, Croatia
[101] Physics Department, Panjab University, Chandigarh, India
[102] Physics Department, University of Cape Town, Cape Town, South Africa
[103] Physics Department, University of Jammu, Jammu, India
[104] Physics Department, University of Rajasthan, Jaipur, India

JHEP09(2017)032

[105] *Physikalisches Institut, Eberhard Karls Universität Tübingen, Tübingen, Germany*
[106] *Physikalisches Institut, Ruprecht-Karls-Universität Heidelberg, Heidelberg, Germany*
[107] *Physik Department, Technische Universität München, Munich, Germany*
[108] *Purdue University, West Lafayette, Indiana, United States*
[109] *Research Division and ExtreMe Matter Institute EMMI, GSI Helmholtzzentrum für Schwerionenforschung GmbH, Darmstadt, Germany*
[110] *Rudjer Bošković Institute, Zagreb, Croatia*
[111] *Russian Federal Nuclear Center (VNIIEF), Sarov, Russia*
[112] *Saha Institute of Nuclear Physics, Kolkata, India*
[113] *School of Physics and Astronomy, University of Birmingham, Birmingham, United Kingdom*
[114] *Sección Física, Departamento de Ciencias, Pontificia Universidad Católica del Perú, Lima, Peru*
[115] *SSC IHEP of NRC Kurchatov institute, Protvino, Russia*
[116] *Stefan Meyer Institut für Subatomare Physik (SMI), Vienna, Austria*
[117] *SUBATECH, IMT Atlantique, Université de Nantes, CNRS-IN2P3, Nantes, France*
[118] *Suranaree University of Technology, Nakhon Ratchasima, Thailand*
[119] *Technical University of Košice, Košice, Slovakia*
[120] *Technical University of Split FESB, Split, Croatia*
[121] *The Henryk Niewodniczanski Institute of Nuclear Physics, Polish Academy of Sciences, Cracow, Poland*
[122] *The University of Texas at Austin, Physics Department, Austin, Texas, United States*
[123] *Universidad Autónoma de Sinaloa, Culiacán, Mexico*
[124] *Universidade de São Paulo (USP), São Paulo, Brazil*
[125] *Universidade Estadual de Campinas (UNICAMP), Campinas, Brazil*
[126] *Universidade Federal do ABC, Santo Andre, Brazil*
[127] *University of Houston, Houston, Texas, United States*
[128] *University of Jyväskylä, Jyväskylä, Finland*
[129] *University of Liverpool, Liverpool, United Kingdom*
[130] *University of Tennessee, Knoxville, Tennessee, United States*
[131] *University of the Witwatersrand, Johannesburg, South Africa*
[132] *University of Tokyo, Tokyo, Japan*
[133] *University of Tsukuba, Tsukuba, Japan*
[134] *Université de Lyon, Université Lyon 1, CNRS/IN2P3, IPN-Lyon, Villeurbanne, Lyon, France*
[135] *Université de Strasbourg, CNRS, IPHC UMR 7178, F-67000 Strasbourg, France, Strasbourg, France*
[136] *Università degli Studi di Pavia, Pavia, Italy*
[137] *Università di Brescia, Brescia, Italy*
[138] *V. Fock Institute for Physics, St. Petersburg State University, St. Petersburg, Russia*
[139] *Variable Energy Cyclotron Centre, Kolkata, India*
[140] *Warsaw University of Technology, Warsaw, Poland*
[141] *Wayne State University, Detroit, Michigan, United States*
[142] *Wigner Research Centre for Physics, Hungarian Academy of Sciences, Budapest, Hungary*
[143] *Yale University, New Haven, Connecticut, United States*
[144] *Yonsei University, Seoul, South Korea*
[145] *Zentrum für Technologietransfer und Telekommunikation (ZTT), Fachhochschule Worms, Worms, Germany*

JHEP09(2017)032